CHARLES UNIVERSITY
Faculty of science

Study programme: Clinical and toxicological analysis
Branch of study: Clinical and toxicological analysis

Študíjny program: Klinická a toxikologická analýza
Študíjny obor: Klinická a toxikologická analýza

Svetlana Kurucová

Heterogeneous Catalysis of Terpenoid Redox Reactions
Heterogénna Katalýza Redoxných Reakcii Terpenoidov

Bachelor´s thesis
Bakalárska práca

Supervisor: Ing. Jan Přech, Ph.D.
Školiteľ: Ing. Jan Přech, Ph.D.

Consultant: Mgr. Mariya Shamzy, Ph.D.
Konzultant: Mgr. Mariya Shamzy, Ph.D.

Prague, 2021

I declare that I worked on this thesis solely by myself and that I cited all references used. This work or a substantial part of it was not used to obtain a different or the same academic degree.

In Prague, 18.06.2021 Svetlana Kurucová

Acknowledgement

I would like to thank my supervisor Ing. Jan Přech, Ph.D. for his help, guidance and patience, as well as my consultant Mgr. Mariya Shamzy, Ph.D. My thanks also belogs to Prof. Jiří Čejka and his research group for their support, help in solving problems and measurements of nitrogen absorption (Mgr. Martin Kubů, Ph.D.), ultraviolet-visible spectra (Jin Zhang) and infrared spectra (Mgr. Kinga Maria Golabek, Ph.D.). I would also like to thank my family and friends for their support during my studies.

Abstract

Heterogeneous catalysts for Meerwein-Ponndorf-Verley (MPV) reduction of ketones and aldehydes are investigated due to issues connected with water sensitivity and separation problems of homogeneous catalysts. During MPV reduction, a hydrogen atom is transferred from the sacrificial alcohol onto the carbonyl group of the ketone/aldehyde forming corresponding alcohol. Tin and zirconium containing zeolites are active catalysts in this hydrogen transfer reaction. However, when using conventional 3D zeolites in the reduction of bulky molecules, e.g., terpenoid compounds, problems with active site accessibility for these bulky reactants may arise. The use of 2D pillared zeolites may represent a solution to the diffusion problem. Silica metal-oxide pillars increase the distance between individual layers of a 2D (lamellar) zeolite and thus improve the active site accessibility. 2D catalysts were prepared by pillaring a parent lamellar pure-Si MFI with a mixture of tetraethyl orthosilicate and Zr (IV) isopropoxide or Sn (IV) isopropoxide, while conventional 3D zeolites were synthesised hydrothermally. The activity of Sn and Zr containing pillared catalysts was compared with the activity of the 3D MFI and beta zeolites in MPV reduction of furfural and citronellal. The 2D zeolites, however, did not facilitate the reaction as expected. Isopulegol (in case of citronellal reduction) and products of acetalisation (in all cases) were detected when using the pillared catalysts as well as 3D MFI zeolites instead of desired alcohols. The catalyst giving the highest conversion of furfural (42 %) is Zr-BEA, while Zr-Pl-MFI-a gave the highest conversion of citronellal (52 %). The highest yield of the desired products (furfuryl alcohol and citronellol) was also obtained when using the Zr-BEA as the catalyst (35% for furfuryl alcohol and 28 % for citronellol).

Abstrakt

Heterogénne katalyzátory pre Meerwein-Ponndorf-Verley (MPV) redukciu ketónov a aldehydov sú skúmané kvôli problémom homogénnych katalyzátorov spojených s citlivosťou na obsah vody a s ťažkosťami so separáciou. Atóm vodíku je počas MPV redukcie prenesený z molekuly obetného alkoholu na karbonylovú skupinu ketónu/aldehydu, pričom vzniká príslušný alkohol. Zeolity obsahujúce cín a zirkónium sú katalyzátory aktívne v tejto reakcii, počas ktorej dochádza k prenosu vodíku. Avšak, pri používaní 3D zeolitov v redukcii objemných molekúl, napr. terpenoidných zlúčenín, môžu vzniknúť problémy s dostupnosťou aktívnych miest pre tieto objemné reaktanty. Riešením vzniknutých difúznych problémov môžu byť 2D pilierované zeolity. Piliere z oxidu kremičitého a oxidu kovu zväčšia vzdialenosť medzi jednotlivými vrstvami 2D (vrstevnatého) zeolitu a tým sa zlepší dostupnosť aktívnych miest. 2D katalyzátory boli pripravené pilierovaním materského vrstevnatého pure-Si MFI so zmesou tetraorto etylsilikátu a isopropoxidu zirkoničitého alebo isopropoxidu ciničitého, kým 3D zeolity boli syntetizované hydrotermálnou metódou. Aktivita pilierovaných zeolitov obsahujúcich Sn a Zr bola porovnaná s aktivitou 3D MFI a beta zeolitov v MPV redukcii furfuralu a citronelalu. Avšak 2D zeolity neurýchľujú reakciu tak, ako sme predpokladali. Namiesto žiadúcich alkoholov bol detekovaný isopulegol (v prípade citronelalu) a produkty acetalizácie (vo všetkých prípadoch) pri použití pilierovaných katalyzátorov a 3D MFI zeolitov. Katalyzátor poskytujúci najvyššiu konverziu furfuralu (42 %) je Zr-BEA, kým Zr-Pl-MFI-a poskytol najvyššiu konverziu citronelalu (52 %). Najvyšší výťažok žiadúcich produktov (furfuryl alkoholu a citronelolu) bol opäť dosiahnutý pri použití Zr-BEA ako katalyzátoru (35 % pre furfuryl alkohol a 28 % pre citronelol).

Contents

List of abbreviations

a.u.	Arbitrary Units
BET	Brunauer-Emmett-Teller
F	Kubelka-Munk Function
FID	Flame Ionisation Detector
FT-IR	Fourier-Transform Infrared Spectroscopy
GC	Gas Chromarography
GC-MS	Gas Chromatography-Mass Spectrometry
IR	Infrared
IZA	International Zeolite Association
MPV	Meerwein-Ponndorf-Verley
NIST	National Institute of Standards and Technology
S	Selectivity
$\mathbf{S_{ext}}$	External Surface Area
SDA	Structure Directing Agent
SEM	Scanning Electron Microscopy
Si/M	Silicon to metal molar ratio
t	Time
TEAOH	Tetraethylammonium hydroxide
TEOS	Tetraethyl orthosilicate
TPAOH	Tetrapropylammonium hydroxide
UV-Vis	Ultraviolet-Visible Spectroscopy
$\mathbf{V_{micro}}$	Micropore Volume
$\mathbf{V_{tot}}$	Total Pore Volume
X	Conversion
XRD	X-ray Diffraction
Y	Yield

1 Introduction

Meerwein-Ponndorf-Verley (MPV) reduction of carbonyl compounds is a highly selective hydrogen transfer reaction. The reduction requires only mild conditions when homogeneously catalysed. Due to separation problems and sensitivity to water, heterogeneous catalysts were also developed for MPV reduction and are further discussed in this thesis.[1] The catalyst must contain metal Lewis acid sites in order to be active in MPV reduction. Such catalysts are e.g. Sn and Zr containing zeolites. Zeolites are widely used as catalysts, as well as adsorbents and ion-exchangers, due to their regular porosity, adjustable chemical composition and reactivity. There are 253 different zeolite frameworks recognised by the International Zeolite Association (IZA, to 8th December 2020) with pore diameters varying from 0.3 to 1 nm. In contrast, only a small number of zeolites is used in the industry e.g. zeolite Y (FAU[a]), MOR, zeolite beta (*BEA), ZSM-5 (MFI). MFI and zeolite beta studied in this thesis are two of the 5 most frequently used zeolites in the industry. Zr and Sn containing zeolites beta have been previously studied[1–3] as catalysts for MPV reduction. So far the most effective zeolite catalyst for MPV reduction proves to be BEA topology[4] with large pores, whereas MFI topology has not been studied as much in regards to MPV reduction due to its small pore diameter.

When reducing terpenoid compounds, the use of conventional 3D zeolite frameworks may lead to problems with bulky reactant processing. The pore diameter may be smaller than the size of the substrate molecule (even when using large-pore zeolite like zeolite beta) and thus the reaction proceeds only on external active sites. 2D zeolites (see Chapter 2.2.1) may eliminate such problems since they provide easier active site accessibility. Pillaring is a simple way to keep individual layers of a 2D zeolite apart preserving the large interlayer space. Silica metal-oxide pillaring (see chapter 2.2) also enables post-synthesis incorporation of heteroatoms – active sites – into the catalyst. The large interlayer space increases, preserved by the pillaring, provides easier access to active sites for bulky reactants while creating new active sites.

The aims of this thesis are as follows:

- To synthesise Zr and Sn containing zeolites with easily accessible active sites using the silica-metal oxide pillaring concept

[a] FAU, MOR, *BEA, MFI - Three letter codes for specific zeolite frameworks assigned by the IZA[27]

- To compare the pillared zeolites with those having conventional 3D frameworks (zeolite beta and MFI) in terms of characterization and catalytic activity in MPV reduction of furfural and citronellal with 2-propanol
- To compare the prepared Sn containing catalysts with the prepared Zr containing catalysts in the MPV reduction of furfural and citronellal with 2-propanol

2 Theoretical Part

A catalyst is a substance that increases the rate of a chemical reaction without being consumed. Although thermodynamics of the reaction remains unchanged, the mechanism changes. A heterogeneous catalyst is present in a different phase than the reactants – typically it is a solid. Therefore, the reaction takes place on the catalyst's surface.[5] On one hand, a heterogeneous catalyst can be easily separated from the reaction mixture. On the other hand, only the surface active sites are accessible for the reactants. In contrast, homogeneous catalysts, which are present in the same phase as reactants, may be difficult to separate from the reaction mixture, but, on the other hand, all the active sites are available. The surface area of a heterogeneous catalyst may be increased by lowering the particle size or introducing porosity to the catalyst. Moreover, the pores enable the reactants to reach active sites that may be present inside the catalyst structure. Generally, the mechanism of a heterogeneously catalysed reaction consists of 7 steps. The first step is external diffusion of the reactants to the surface of the catalyst, followed by internal diffusion of reactants through the pores of the catalyst to an active site. The reactants then adsorb on the active site and transformation to products takes place. The products of the reaction desorb from the active site, internally diffuse out of the pores and finally externally diffuse from the catalyst surface. External diffusion, internal diffusion and surface reaction are factors affecting the rate of a reaction. The effect of external diffusion can be easily eliminated by stirring the reaction mixture more vigorously when using a batch apparatus or by using appropriate reaction mixture flow rate when working in a flow apparatus. The effect of internal diffusion on the rate of a reaction can be limited by decreasing the crystal size, as well as changing the pore size. Eliminating both external and internal diffusion enables us to work in a regime, where the rate-determining step is the chemical reaction. Omitting the diffusion phenomena, we distinguish three fundamental mechanisms of a heterogeneously catalysed reaction: Langmuir-Hinshelwood, Rideal-Eley and Mars-Van-Krevelen mechanism. According to the Langmuir-Hishelwood mechanism the chemical reaction occurs after both reactants adsorb to the catalyst surface. Rideal-Eley mechanism states that a reactant in the gas phase reacts with the other adsorbed reactant .[6] Mars-Van-Krevelen mechanism applies when a product of the reaction contains a part of the catalyst's lattice element (e.g. Oxygen) as a result of the catalyst oxidation or reduction. Later, reactant flows are switched and the catalyst is reduced or oxidised back to its active state. In other words, the adsorption of the reactants is separated in time.[7]

Due to easy manipulation with the catalyst, heterogeneous setup is widely used in the industry. Mainly, the production of bulk chemicals (e.g. Ammonia synthesis) and fuels (e.g. fluid catalytic cracking) are of the most important heterogeneously catalysed processes. Heterogeneous catalysis also plays an important role in environmental protection (e.g. deNO_x processes) and potentially it may represent a key to CO_2-neutral processes.[8]

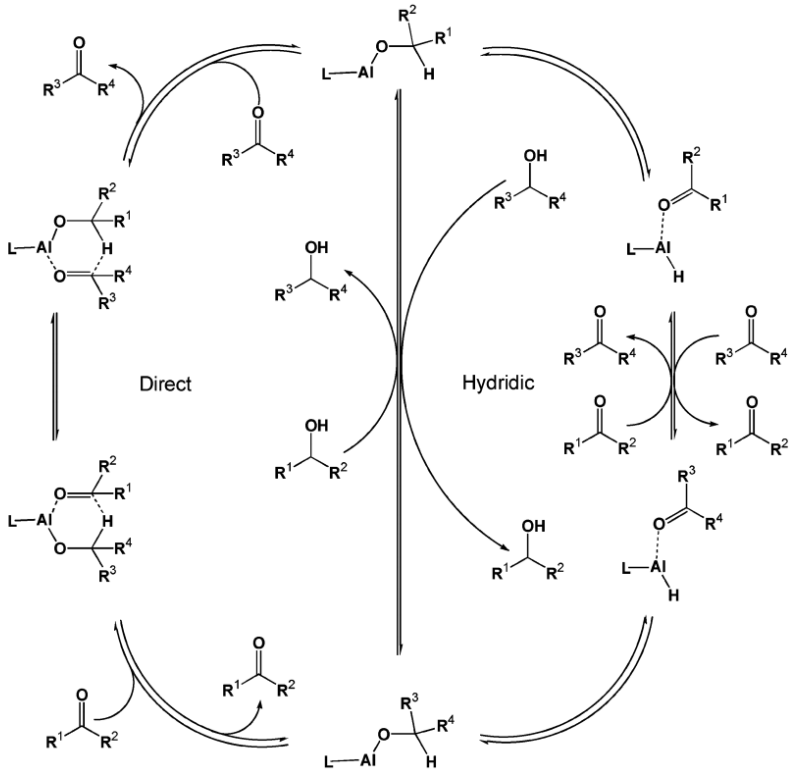

Figure 1: Possible mechanisms of Al-alkoxide catalysed MPV reduction. Right: Direct hydrogen transfer pathway. Left: Hydridic pathway. Adapted from Cohen et al.[9]

2.1 Meerwein-Ponndorf-Verley reduction

Meerwein-Ponndorf-Verley[10] reduction is a hydrogen transfer reaction between a carbonyl compound and secondary alcohol resulting in the formation of corresponding alcohol from the carbonyl compound and a ketone. Oppenauer oxidation is the reversed process to MPV reduction. Due to its high chemoselectivity and mild reaction conditions[11], both MPV reduction and Oppenauer oxidation are suitable for organic synthesis and biomass processing. Metal alkoxides, such as aluminium isopropoxide, were the first catalysts of the MPV reduction. The MPV reduction is believed to proceed according to a direct hydrogen transfer pathway[12], though other mechanisms have also been proposed: a hydridic[9] and a radical mechanism[13]. The direct

hydrogen transfer pathway proposes the formation of a six-membered cyclic transition state, in which both the carbonyl compound and the alcohol are coordinated to the metal atom of the catalyst as is shown in Figure 1. Whereas according to the hydridic mechanism a metal hydride species is formed and the hydride is further passed onto the substrate (Figure 1).[9] In addition to metal alkoxides, a number of other catalysts are active in MPV reduction. When using heterogeneous catalysts, such as hydrotalcites, magnesium oxide, alumina, zirconia, metal alkoxides grafted on mesoporous materials and Al-, Sn- or Zr-substituted zeolites, the hydrogen transfer is most probably performed through the direct mechanism since the C=O bond is activated for MPV reduction only if the carbonyl group is directly coordinated to a metal atom.[14,15] Particularly, tin and zirconium atoms in the zeolite framework, acting as Lewis acid sites due to their vacant d-orbitals, can activate the C=O bond *i.a.* for MPV reduction.[3]

2.2 Zeolites

Zeolites are important heterogeneous catalysts due to their unique morphology, textural properties and acidity. They are crystalline microporous[b] aluminosilicates with a defined system of pores, which results from their crystalline structure. Zeolites consist of TO_4 tetrahedra connected together via oxygen bridges, where the central atom T is Si or Al. Aluminium isomorphously incorporated in the siliceous framework creates strong Brønsted acid sites. Different heteroatoms may be substituted instead of Al, such as 3+ metal ions that also create Brønsted acid sites, although not as strong. Whereas 4+ metal ions act as Lewis acid sites due to vacant d-orbitals. The desired concentration of acid sites may be obtained by varying the Si/M[c] ratio. The defined system of pores provides high surface area as well as defined restriction of the reaction space resulting in so-called shape selectivity[16]. However, some reactants may not be able to enter the catalyst's pores due to their size and thus only external surface active sites (located on the external surface of the crystals) are available. To obtain even higher surface area 2-dimensional (2D, layered, lamellar) zeolites are a great option (see below[17]). In addition, 2D zeolites provide improved accessibility of active sites, which is desirable when using bulky reactants. Furthermore, zeolites conform to the 'green chemistry' concept, since they are easily separated from the reaction mixture, can be used multiple times and do not contain heavy metals.[18,19] Moreover, their chemical composition and macroscopic reactivity can be compared to sand. There are 253 zeolite structures recognized by IZA (to 8th December 2020), with

[b] According to IUPAC, microporous materials have pores with diameter smaller than 2 nm.
[c] M - Metal

different sized cavities, pore systems, and pore diameters. Pore size and dimensionality of pores determine, which substrates can enter their porous structure.

Tetrahedral Sn and Zr atoms isomorphously incorporated in the zeolite frameworks serve as the active sites for MPV reduction (see above). Extra-framework Sn or Zr have no activity.[2] However, incorporating a Sn or Zr atom into the zeolite framework is a challenging task. There are several ways how to achieve it. Hydrothermal synthesis is the most straightforward way of preparing Zr- and Sn-containing zeolites; however, the need for HF use is a big drawback. In addition, long synthesis times are caused by neutral pH that prevents the precipitation of metal oxides from metal precursors.[1,3] In order to avoid using HF, another option is to incorporate Sn and Zr post-synthesis, for example, by grafting[20], wet impregnation[3], chemical vapour deposition[21], solid-state ion-exchange[22] and silica-metal-oxide pillaring[23]. In silica metal-oxide pillaring, a layered pure-Si zeolite is pillared with a mixture of TEOS and M-alkoxide.[23] However, silica metal-oxide pillaring may be used only on 2D zeolites, while other post-synthesis incorporation techniques can be used on both 2D and 3D zeolites. On one hand, post-synthetic incorporation is a simple way of incorporating Zr and Sn into the framework. On the other hand, the majority of MPV active sites are present on the surface of the catalyst.

2.2.1 Layered (2D) Zeolites

Besides the nature and strength of active sites present on zeolites, overall surface area (most commonly expressed as BET area), external surface area, pore diameter and pore volume are other characteristics that influence the overall efficiency of a catalyst. When using bulky reactants such as terpenoids, microporous catalysts provide low accessibility of active sites, which results in overall low efficacy of the catalyst. In order to improve the access to the active sites, either a different zeolite structure with larger pores or a 2D zeolite may be chosen. Conventional 3D zeolite crystals have all three dimensions of the same (or similar) order, whereas 2D zeolite crystals have one of the dimensions reduced to the size of a unit cell. Individual layers of 2D zeolites are of approximately a unit cell thickness. Layered zeolites may be prepared in three ways shown in Figure 2. Firstly, by hydrothermal synthesis, where a 3D zeolite is formed through a layered zeolite precursor (e.g. MCM-22P). After calcination, the layers of the precursor that are intercalated with a structure-directing agent (SDA) topotactically condense. Another way how to prepare a lamellar zeolite is by using a specially designed organic SDA. The SDA consists of a polar part, which promotes the crystallisation of the zeolite framework while the non-polar tail restricts the growth in one direction.[24]. Disassembling a 3D

zeolite into a corresponding layered zeolite is the third way of synthesizing 2D zeolites. However, the starting 3D material must contain a sufficient amount of a sensitive dopant that is located in specific positions (e.g. Germanium in double-4-ring units, which is hydrolytically unstable).[25,26]

In order to prevent the layers from collapsing and preserve or increase the interlayer void space, the original lamellar structure may be modified by swelling and organic or inorganic pillaring.[17] Overall, these modifications expand the interlayer distance, thus providing higher surface area and lower diffusion limitations when working with bulky reactants. The layered swollen structure may also be stabilised, delaminated or transformed into a colloidal suspension.

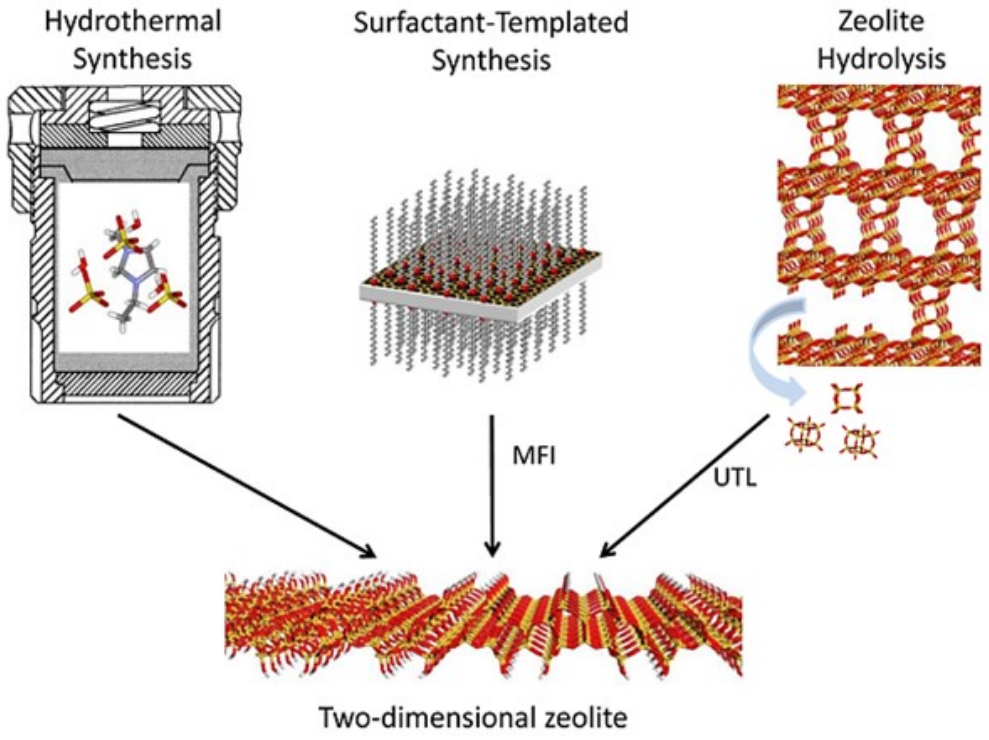

Figure 2: Three ways to synthesise 2D zeolites. Reprinted with permission from W. J. Roth et al.[17]

2.2.2 MFI

Aluminosilicate MFI zeolite (ZSM-5) is one of the most important zeolites used in petrochemistry. It has been accepted by the IZA in 1978. MFI has 10-ring pores with diameter 5.3 and 5.6 Å that form 3D-connected straight and zig-zag channels. The structure of the zeolite framework is shown in Figure 3. The MFI zeolite can be also prepared with other heteroatoms

but Al. Of these, for instance, Ti-MFI (Titanium silicalite 1) is a selective oxidation catalyst, which has been commercialised as well. In this thesis, we apply Sn and Zr containing catalysts.

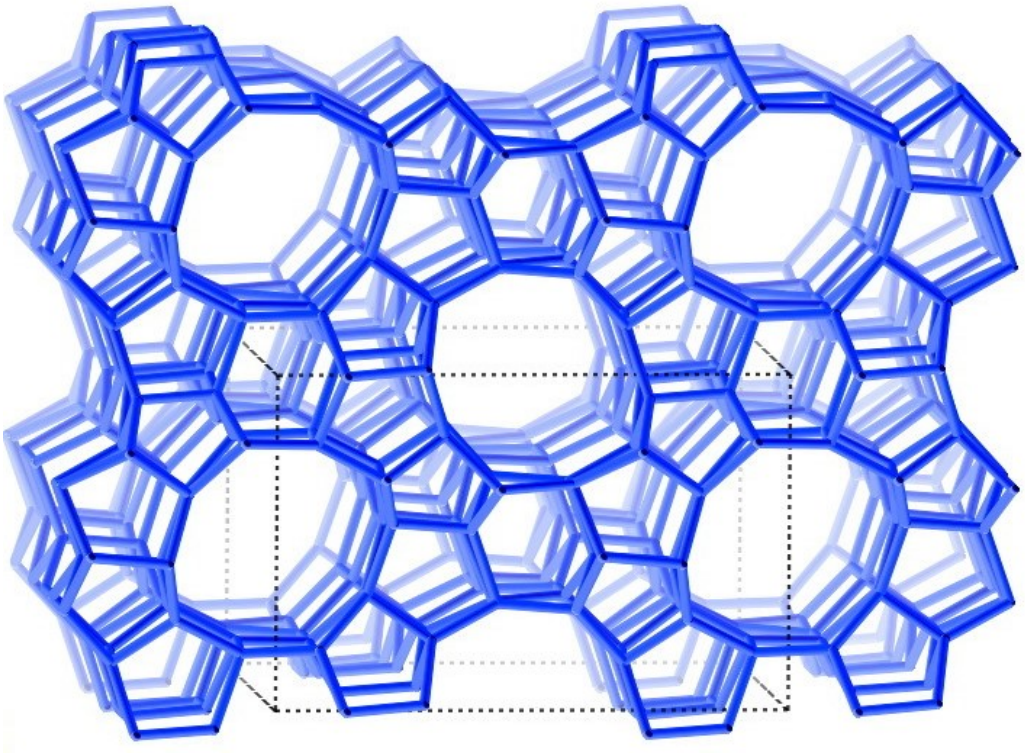

Figure 3: MFI Framework with its unit cell marked by the dotted lines. Adapted from IZA Database.[27]

2.2.3 *BEA

Zeolite beta is also one of the 'big five' zeolites used in industry. Zeolite beta is a combination of 2 or 3 polymorphs A, B and C; the structure of polymorph A is shown in Figure 4. It has 12-ring pores with diameter 6.7 Å, which form 3D connected channels that are advantageous when working with bulky reactants. It has been accepted by the IZA in 1992. Zeolite beta is used as a catalyst in cracking, hydrocracking, alkylation, acylation and isomerisation processes.[28]

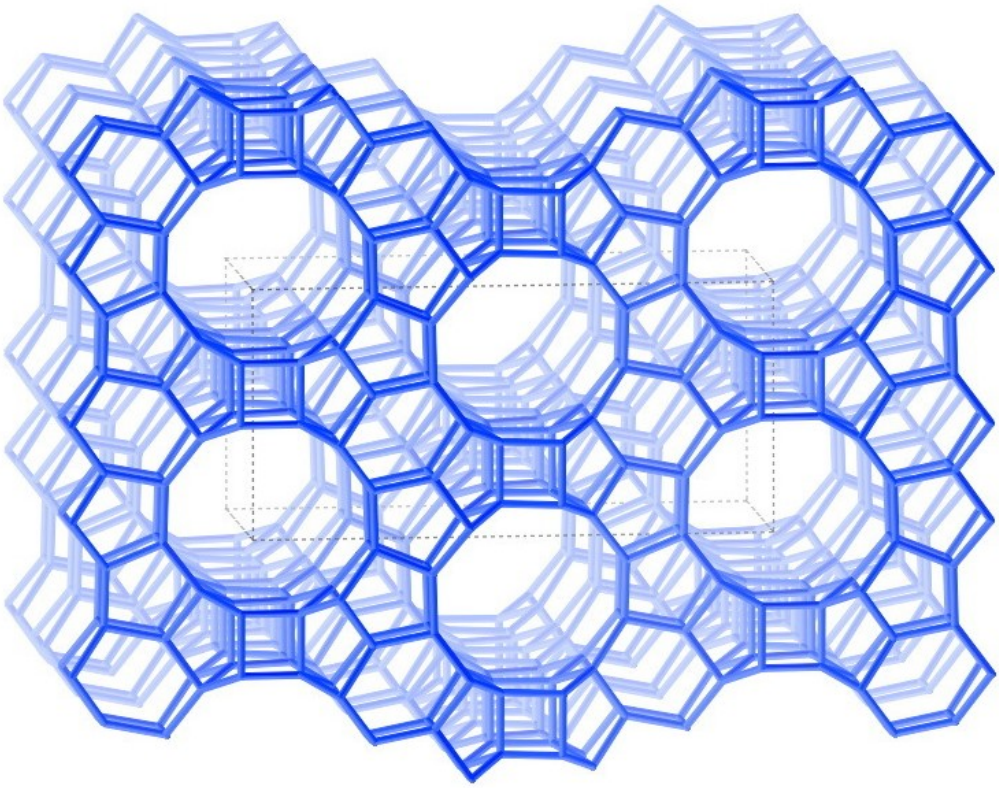

Figure 4: Zeolite beta framework – polymorph A with its unit cell marked by the dotted lines. Adapted from IZA Database.[27]

2.3 Characterisation techniques

The most important characteristics of a zeolite are its framework structure, (external) surface area, total pore volume, micropore volume, the shape and size of the zeolite crystals, the number and nature of acid sites. In addition, when incorporating heteroatoms into the framework, it is important to check if the heteroatom is a part of the framework. These attributes define the studied material and thus its performance in the chosen field (e.g. catalysis). In order to determine the materials studied in this thesis, the techniques further described were used.

2.3.1 X-ray powder diffraction

X-ray diffraction (XRD) is a technique used to determine the atomic structure of a crystalline sample. The incident beam of X-rays is diffracted into different directions depending on the structure of the crystal. The structure may be calculated based on the intensity and angle of diffracted X-rays. Powder XRD (powder XRD phase analysis) gives a one-dimensional diffractogram as a result of crystals in the powder being oriented in different ways. Powder XRD provides rapid identification or confirmation of a zeolite structure. Each zeolite structure has its own unique diffraction pattern. For simple identification of the zeolite structure, its

diffraction pattern is compared to those in IZA database[27]. In XRD the crystal framework of zeolites causes the incident beam to diffract on its planes. The diffraction pattern is a result of constructive and destructive interferences of diffracted beams at certain angles which correspond to Bragg's equation (1), where λ is the wavelength of the incident beam, d is interplanar distance, Θ is the angle between the incident beam and the crystalline plane and where n is a natural number.[29]

$$n\lambda = 2d \sin\theta \quad (1)$$

2.3.2 Physisorption analysis of textural properties

Textural properties such as external surface area, micropore area, total pore volume, micropore volume, are important assets of catalysts. These parameters are determined from gas physisorption isotherms. Adsorption isotherm shows how the amount of adsorbed gas changes with pressure at a constant temperature. If the temperature is lower than the adsorbate's critical temperature then the adsorption isotherm may be expressed by equation (2) where n is the number of moles of the adsorbed gas, m is the mass of the sample, p/p^0 is relative pressure and T is temperature.

$$\frac{n}{m} = f\left(\frac{p}{p^0}\right)_T \quad (2)$$

Nitrogen and argon are commonly used as adsorbates in these analyses and measurements are performed at their boiling point temperatures (-196°C and -186°C, respectively). Nitrogen is common for its easy accessibility and price whereas argon provides more accurate data while characterising microporous samples.[30] The adsorbate molecules are physisorbed on the surface of the catalyst at low temperature, which means forces binding the gas molecules to the catalyst are weak Van der Waals forces regardless of the characteristics of the catalyst's surface and active sites. The simplest plausible model of adsorption is described by Langmuir isotherm. This model is based on several presumptions:

- the adsorbent surface is homogeneous
- 1 molecule of adsorbed gas occupies 1 adsorption site
- the adsorbed molecules do not interact with each other
- the adsorption is completed when a monolayer is formed.

The surface area may be easily calculated if the area occupied by 1 adsorbate molecule is known - that is if the physisorbed gas forms a monolayer. However, in reality, multilayer adsorption occurs, therefore one of the presumptions of the Langmuir model is not fulfilled. A model that assumes multilayer formation is the BET (Brunauer-Emmett-Teller) adsorption model, which at first enables to calculate the amount of gas corresponding to a monolayer from the real adsorbed amount. Gas molecules condense in pores due to a bigger force pulling the gas inside the pores. Pore shape and pore distribution change the shape of the adsorption isotherm. [31]

2.3.3 Ultraviolet-visible reflectance spectroscopy

Incorporating of certain heteroatoms (i.a., Ti, Zr, Sn) into the zeolite framework can be verified using ultraviolet-visible spectroscopy (UV-Vis) in diffuse reflectance mode. It is used to verify the incorporation of the metal into the framework. In conventional spectroscopy abiding by Lambert-Beer law, light scattering and reflection do not decrease light intensity. However, diffuse reflectance spectroscopy uses Kubelka-Munk function because opaque and strongly scattering materials reflect light diffusively. The reflecting power is affected by the materials ability to absorb light. The relationship between reflecting power and absorption coefficient is described by the Kubelka-Munk function.[32] A spectrum is obtained by measuring the value of Kubelka-Munk function at selected wavelengths. Framework Sn provides a maximum at ~220 nm, while extra-framework Sn-species absorb at 260-280 nm.[33] Similarly, Zr atoms incorporated into the framework absorb at 205-215 nm, whereas ZrO_2 has a maximum at ~240 nm.[34]

2.3.4 Scanning electron microscopy

Scanning electron microscopy (SEM) is a technique used to determine the crystal size and morphology of zeolites. An SEM image only shows what the surface of our sample looks like, it cannot expose the inner structure. A beam of electrons is either elastically scattered on the surface of a zeolite or a part of their energy is absorbed by electrons in the studied material. The absorbed energy causes the sample to eject secondary electrons. Both secondary and back-scattered electrons are detected. The intensity of the detected electrons and the angle under which they were emitted or reflected into the detector is used to form an image of the surface.[35] Typical accelerating voltage used in SEM of zeolites is 5-8 kV, which gives us resolution of a few nanometres.

2.3.5 Fourier-transformation infrared spectroscopy

Fourier-transform infrared spectroscopy (FT-IR) can be used to observe functional groups with characteristic vibrations (e.g., silanol groups) or to analyse the nature, strength and amount of acid sites in the zeolite framework. The sample is irradiated with IR radiation. The radiation with energy corresponding to the vibrational energy of the bonds present in the zeolite framework. The radiation that was not absorbed by the sample passes through the interferometer to a detector. The signal from the detector is sent to the computer, where it is converted into a spectrum using Fourier-transformation.[36] In this thesis, FT-IR was used to analyse the amount of silanol groups on the surface of selected zeolites. Free silanol groups, that do not interact with any other groups and are not a part of oriented silanol groups, that are connected by hydrogen bonds, absorb at 3747 cm^{-1}. A broad band at 3650-3500 cm^{-1} points to the presence of oriented silanol groups connected by hydrogen bonds. Terminal silanols - silanol groups at the end of oriented silanol groups, whose hydrogen atom does not form a hydrogen bond with other silanol groups, absorb at 3740-3700 cm^{-1}.[37,38]

3 Working hypothesis

Catalytic activity of a Zr- and Sn- zeolite-based MPV catalysts is determined by surface area, pore diameter, and type, number and accessibility of active sites. Thus, we decided to investigate the use of zirconia-silica and tin-silica pillared zeolites as MPV reduction catalysts.

It is known that the large-pore zeolite beta will have higher activity in MPV reduction of furfural and citronellal than MFI zeolite that has smaller pores. Nevertheless, 2-dimensional form of MFI zeolite, the catalyst prepared by silica-metal oxide pillaring, should have better active site accessibility in comparison to conventional MFI and beta zeolites and therefore the pillared zeolites should be more active in MPV reduction of furfural and citronellal. In addition, the difference between Zr and Sn based catalysts will be investigated.

4 Experimental part

4.1 List of used chemicals

Table 1: List of used chemicals.

Name	Purity	Manufacturer	Abbreviation
2-propanol	100 %	Lach-ner	
Citronellal	≥ 95%	Sigma Aldrich	
Furfural	99%	Sigma Aldrich	
Glacial acetic acid	100%	MERCK	
Hydrofluoric acid	40%	VWR Chemicals	
Ludox HS-40	40%	Sigma Aldrich	
Mesitylene	98+%	Alfa Aesar	
Sodium hydroxide	99%	MERCK	
Tetraethyl orthosilicate	100%	VWR Chemicals	TEOS
Tetraethylammonium hydroxide	40%	Sigma Aldrich	TEAOH
Tetrapropylammonium hydroxide	1M	MERCK	TPAOH
Tin(IV)chloride pentahydrate	98%	Sigma Aldrich	
Tin(IV)isopropoxide	99.99%	Sigma Aldrich	
Zirconium(IV)chloride	≥ 98%	Sigma Aldrich	
Zirconium(IV)isopropoxide	99.9%	Sigma Aldrich	
Zirconyl chloride octahydrate	98%	Sigma Aldrich	

4.2 Synthesis of the catalysts

Zr-BEA, Zr-MFI, and Sn-MFI were synthesised using the hydrothermal synthesis method. To prepare Zr-BEA according to Wang et al.[3], 28.16 g of TEOS were mixed with 27.82 g of 40% TEAOH in a 100ml Teflon beaker, which also serves as an autoclave liner and stirred for 2 hours using a magnetic stirring bar. Afterwards, an aqueous solution of $ZrOCl_2 \cdot H_2O$ consisting of 0.87 g of $ZrOCl_2 \cdot H_2O$ and 3.86 g of deionised water was added dropwise. After

3 hours of further stirring, 3,8 g of 40% HF were added into the gel followed by 0.28 g of BEA seeds with Si/Al = 382, kindly provided by Mgr. Ondřej Veselý, in 2.7 g deionised water. The final gel molar composition was 1 SiO_2:0.02 ZrO_2:0.56 TEAOH:0.56 HF:10.5 H_2O. The Teflon liner containing the synthesis gel was put into a stainless-steel autoclave. The autoclave was placed inside a drying oven for 20 days at 140 °C. After the given time, the autoclave was cooled down and the obtained solid product was filtered on a Büchner funnel, washed with deionised water and dried at 60 °C. Calcination to remove the SDA from pores was performed at 580 °C with heating rate 2 °C/minute for 10 hours. A chamber furnace (350x250x500 mm chamber size) was used. The furnace was equipped with an Ht40P programmable thermoregulator. Sn-BEA was synthesised hydrothermally following reference[39] and supplied by Mgr. Mariya Shamzy, Ph.D. Imp-Sn-BEA was prepared by degermanation followed by impregnation with $SnCl_4$ by Ing. Jan Přech, Ph.D similarly to a procedure described in reference[40].

To synthesise Zr-MFI, 0.58 g of zirconium isopropoxide was dissolved in 5.03 g of deionised water and added to a Teflon liner containing 15.66 g of TEOS. Secondly, 25 ml of 1M TPAOH were added into the mixture dropwise and stirred for 1 hour. Afterwards, 29 ml of deionised water were added to the mixture and the ethanol formed upon hydrolysis were evaporated at 60 °C in an oil bath. The final reaction gel had the molar composition of 1 SiO_2:0.02 ZrO_2:0.33 TPAOH:40 H_2O. The crystallisation took place in a stainless steel autoclave inside a drying oven equipped with a tumbling rack at 150 °C, 60 rpm for 5 days. The obtained solid was filtered on a Büchner funnel, washed with deionised water and dried at 60 °C. The calcination was performed at 330 °C for 3 hours and 550 °C for 7 hours using a heating rate of 2 °C/minute.[41]

Sn-MFI-a was prepared according to N. G. Vargas et al.[42] 0.43 g of $SnCl_4 \cdot 5H_2O$ was added into a Teflon liner containing 1.42 g of NaOH dissolved in 17.3 g of deionised water. After 15 minutes of stirring, 18.23 g of Ludox HS-40 colloidal silica were added and the mixture was stirred for 20 minutes. Then, 26 ml of 1M TPAOH was added dropwise to the gel. After 1.5 hours, the pH of the mixture was adjusted to 12 using a 50% solution of acetic acid. The final gel had the composition of 1 SiO_2:0.01 $SnCl_4$:0.21 TPAOH:0.3 NaOH:22 H_2O. The Teflon liner with the synthesis mixture was put into a stainless steel autoclave to crystallise at 155 °C, 60 rpm for 6 days in a drying oven equipped with a tumbling rack. The obtained solid material was filtered on a Büchner funnel, washed with deionised water and dried at 60 °C. The sample was calcined at 300 °C for 3 hours, followed by 550 °C for 7 hours with a heating rate

of 2 °C/minute. Sn-MFI-b supplied by Mgr. Mariya Shamzy, Ph.D. was synthesised hydrothermally according to Mal et al.[43]

The pillared MFI zeolites were prepared following a general procedure described in reference[23] from parent pure-Si layered MFI, which was taken from the research group's stock and was prepared earlier according to a modified procedure of Ryoo et al.[44] The parent layered MFI in the as-synthesized form (that means containing the organic SDA) was dispersed in a mixture of TEOS and Sn (IV) isopropoxide or Zr (IV) isopropoxide (1 g of MFI per 10 g of TEOS mixture) in a 50ml round-bottom flask. To prepare Pl-Sn-MFI-a and Pl-Zr-MFI-a the TEOS mixture had a molar ratio of Si/M = 30, while the TEOS mixture used to prepare Pl-Sn-MFI-b and Pl-Zr-MFI-b had a molar ratio of Si/M = 60. The mixture was stirred at 65 °C and after 24 hours it was centrifuged at 3500 rpm for 10 minutes. The liquid above the solid material was disposed of while the solid was dried at ambient temperature for 48 hours. The dry material was hydrolysed in water with 5% of ethanol (100 ml of solution per 1 g of material) in a plastic beaker for 24 hours with continuous stirring. At last, the material was centrifuged at 3500 rpm for 10 minutes, dried at 60 °C and calcined at 550 °C for 10 hours using a heating rate of 2 °C/minute. Pl-Sn-MFI-c and Pl-Sn-MFI-d were kindly provided by Ing. Jan Přech, Ph.D. and synthesised according to the same method as described above.

4.3 Zeolite sample characterisation

The powder XRD diffractograms were measured on a Bruker D8 Advance diffractometer equipped with a Linxeye XE-T detector, using Cu Kα radiation (λ = 0,15406 nm). The zeolite samples were pressed onto a plastic holder. The pillared catalysts were measured in 1-40° 2Θ range in 2000 steps with 0.8 s per step. The 3D zeolite beta and MFI samples were measured in 3-40° 2Θ range in 1775 steps with 0.8 s per step. Lamellar and pillared catalysts are measured from 1-40° 2Θ due to a peak present at 1.5 2Θ that reflects the interlayer distance. This peak is not present in 3D zeolites because the layers are condensed and thus there the powder pattern is measured from 3-40° 2Θ.

The textural properties were determined from nitrogen sorption isotherms collected using Micromeritics 3Flex volumetric surface area analyser. At first, the catalysts were degassed using a turbo molecular pump vacuum (Micromeritics Smart Vac Prep instrument); the samples were heated to 110 °C with a heating rate of 1 °C/minute until the residual pressure reached 13.3 Pa. After maintaining the temperature at 110 °C for 1 hour, the samples were heated to

250 °C for 8 hours using the heating rate of 1 °C/minute. Afterwards, the nitrogen adsorption/desorption was performed at -196 °C. The BET area was determined from adsorption data in the p/p^0 range of 0.05-0.2. The micropore volume and external surface area were evaluated using the t-plot method. The total adsorption volume is equal to the amount of nitrogen adsorbed at p/p^0 = 0.95. The measurements were carried out by Ing. Martin Kubů, Ph.D.

Ultraviolet-visible reflectance spectra were measured by Agilent Cary 4000 UV-VIS spectrometer in the wavelength range of 190-800 nm. $BaSO_4$ was used as a 100% reflectance standard. The measurements were taken by Jin Zhang. The spectra were transformed into absorption spectra using the Kubelka-Munk function.

The FT-IR spectra were recorded with a Nicolet 6700 FT-IR Spectrometer equipped with an AEM module with a resolution of 2 cm^{-1}. The self-supporting wafers (ca. 8-12 mg/cm^{-2}) of the zeolitic materials were pre-treated in situ in quartz IR cell at 450 °C under vacuum conditions for 2 h. The IR-spectra were measured by Mgr. Kinga Maria Golabek, Ph.D.

The morphology of the catalysts was analysed using a scanning electron microscope FEI Quanta 200F equipped with secondary electrons and back-scattered electron detectors. The samples were deposited onto a carbon tape attached to an SEM holder. The images were collected with an accelerating voltage of 8 kV using beam spot size 4.

4.4 Catalytic reactions

Before the catalytic experiment, 100 mg of catalyst were activated at 450 °C for 1.5 hours with a heating rate of 5 °C/minute in a laboratory furnace with a 200x160x400 mm chamber and cooled down in a desiccator. The experiments were performed in a 25 ml round-bottom flask equipped with a reflux condenser, a septum port and a magnetic stirrer heated by an aluminium block placed on a hot plate magnetic stirrer (Starfish™ apparatus). 23 mmol of 2-propanol and 1.3 mmol of internal standard (mesitylene) were added to the solid catalyst in the flask and heated to 70 °C under stirring. The reaction was initiated by the addition of 2.6 mmol of substrate (furfural, citronellal) to the flask. 250µl samples of the reaction mixture were taken every hour and the products were analysed using a gas chromatograph (GC) Agilent 7890B equipped with an autosampler, a DB-5 column (30 m, 0.32 mm, 0.25 µm) and FID detector.

Reaction products were identified using a GC-MS by Thermo Scientific ISQ^{TM} Series Single Quadrupole GC-MS system. The GC-MS system was equipped with a TraceGOLD TG-5MS GC column, electron impact ionisation and a single quadrupole analyser. The range of monitored weight was *m/z* = 40-500. The products were identified by comparison of their mass spectra with the NIST library. In case that the products' spectra did not match with the NIST library, the spectra were interpreted by Ing. Jan Přech, Ph.D.

The conversion of furfural and citronellal was calculated as the ratio of the amount of converted and initial amount of furfural and citronellal (see equation 3, where A_0 is the initial area of aldehyde, A_{STD} is the area of the internal standard at given time and A is the area of aldehyde in given time). The yield of furfuryl alcohol and citronellol was calculated as the ratio of furfural and citronellal converted to their corresponding alcohols and the initial amount of either substrate (see equation 4, where K is coefficient specific for every product and was calculated in calibration – see below). Selectivity was determined as the amount of alcohol formed relative to the amount of converted furfural or citronellal (see equation 5, where Y is yield and X is conversion).

$$X = \frac{\frac{A_0}{A_{STD}} - \frac{A}{A_{STD}}}{\frac{A_0}{A_{STD}}} \tag{3}$$

$$Y = \frac{K \cdot \frac{A}{A_{STD}}}{\frac{A_0}{A_{STD}}} \tag{4}$$

$$S = \frac{Y}{X} \tag{5}$$

4.4.1 GC Calibration

The method of internal standard was used for calibration of the catalytic experiment. A response coefficient K, specific for every product, needed to calculate yield was determined as the ratio of slopes of calibration lines of alcohol and aldehyde. Mesitylene was the internal standard in both reductions of furfural and citronellal. A stock solution containing mesitylene, aldehyde and corresponding alcohol of concentration 50 mg/ml was prepared using 2-propanol as solvent. The stock solution was used to prepare other calibration solutions with concentrations 10, 5, 1 and 0.5 mg/ml. The solutions were analysed by GC by Agilent 7890B. The obtained data were used to plot a graph (see Figure 5).

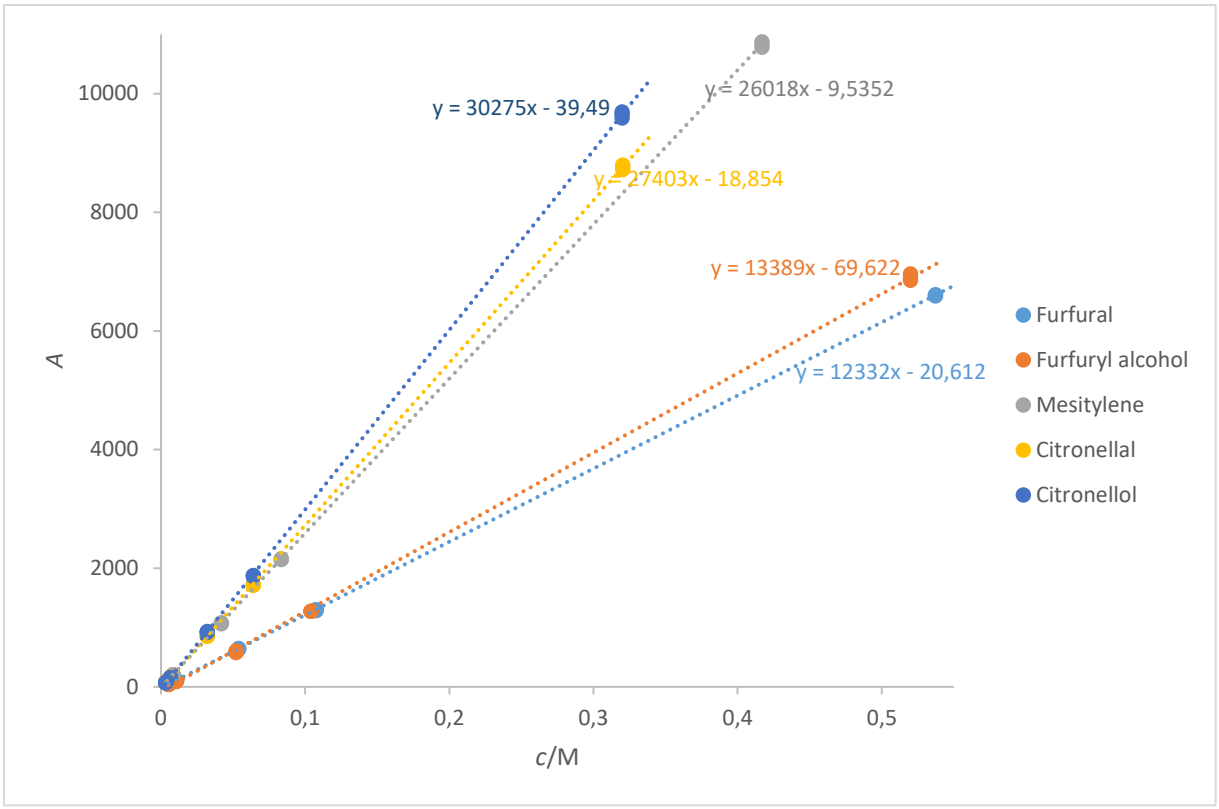

Figure 5: Calibration graph.

5 Results and discussion

The MPV reduction was studied on Zr and Sn containing zeolite-based catalysts. Samples with BEA and MFI topologies were prepared – Zr-BEA, Zr-MFI and Sn-MFI and the catalytic activity of both topologies was compared in MPV reduction of furfural and citronellal. Furthermore, 2D zeolite catalysts were synthesised by silica metal-oxide pillaring of pure-Si lamellar MFI - Zr-Pl-MFI-a, Zr-Pl-MFI-b, Sn-Pl-MFI-a and Sn-Pl-MFI-b. The pillared catalysts were expected to provide better active site accessibility, and thus a higher catalytic activity than 3D zeolites, due to bigger interlayer distances.

5.1 Characterisation of zeolites

The topology of prepared catalysts was confirmed by powder XRD. The XRD pattern has peaks in different positions for every topology depending on its atomic structure. It can be taken as a structure fingerprint. The powder XRD patterns of the synthesised zeolite catalysts are shown in Figure 6 (beta zeolites), Figure 7 (3D MFI zeolites) and Figure 8 (2D zeolites) together with IZA database[27] reference patterns. The broad band at $2\Theta = 7.9°$ indicates that Zr-BEA, Sn-BEA and imp-Sn-BEA consist of 60-70 % of polymorph A[1] and the overall pattern is consistent with those observed before for the zeolite beta samples. All three XRD patterns of the synthesised 3D MFI zeolites correspond to the reference pattern observed for MFI before.

Figure 8 shows XRD patterns of the pillared zeolite samples. Although the peaks of the XRD patterns of the pillared samples have higher intensity, the resolution of individual peaks is worse in comparison to patterns of 3D MFI (compare, e.g., group of peaks between $2\Theta = 23°$ and 25°). Moreover, some peaks are missing in the XRD patterns of 2D zeolites due to the absence of framework growth in one crystallographic direction.[45] The peak at $2\Theta = 1.5°$ present in pillared catalysts XRD patterns reflects the distance between individual zeolite layers. After synthesis, individual zeolite layers are kept apart by molecules of SDA. Due to the molecules of SDA present in the interlayer space, the peak at $2\Theta = 1.5°$ is present in the pattern of a sample before the calcination. During pillaring silica metal-oxide pillars are formed in the interlayer space, thus the peak at $2\Theta = 1.5°$ is preserved after calcination when the SDA is removed. However, its position may vary to some extent since the pillars are amorphous that is less ordered. If the layered zeolite was calcined without the pillaring treatment, the peak at $2\Theta =$

1.5° would disappear, because the interlayer distance would decrease and the order would diminish.

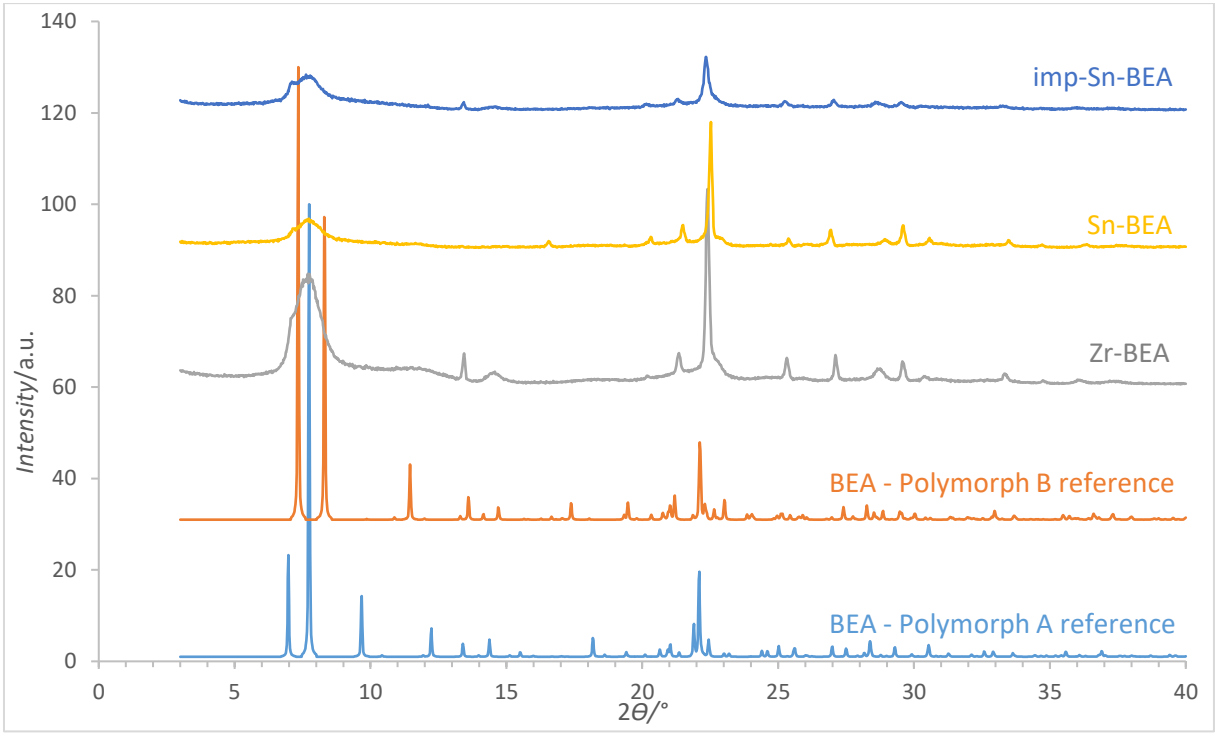

Figure 6: XRD patterns of the synthesised beta zeolites. Patterns for BEA – Polymorph A reference, BEA – Polymorph B reference and are calculated XRD patterns for corresponding zeolites taken from the IZA database.[27]

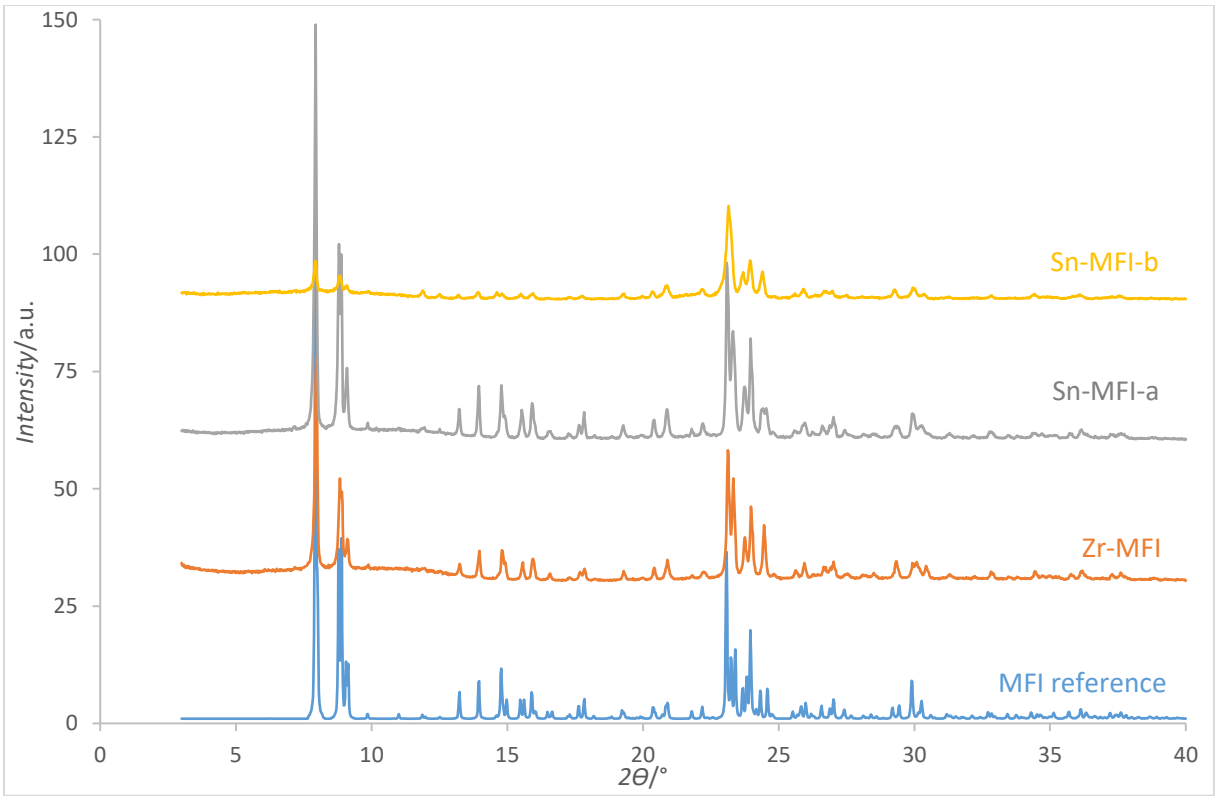

Figure 7:XRD patterns of the synthesised MFI zeolites.MFI reference is a calculated XRD pattern for the corresponding zeolite taken from the IZA database.[27]

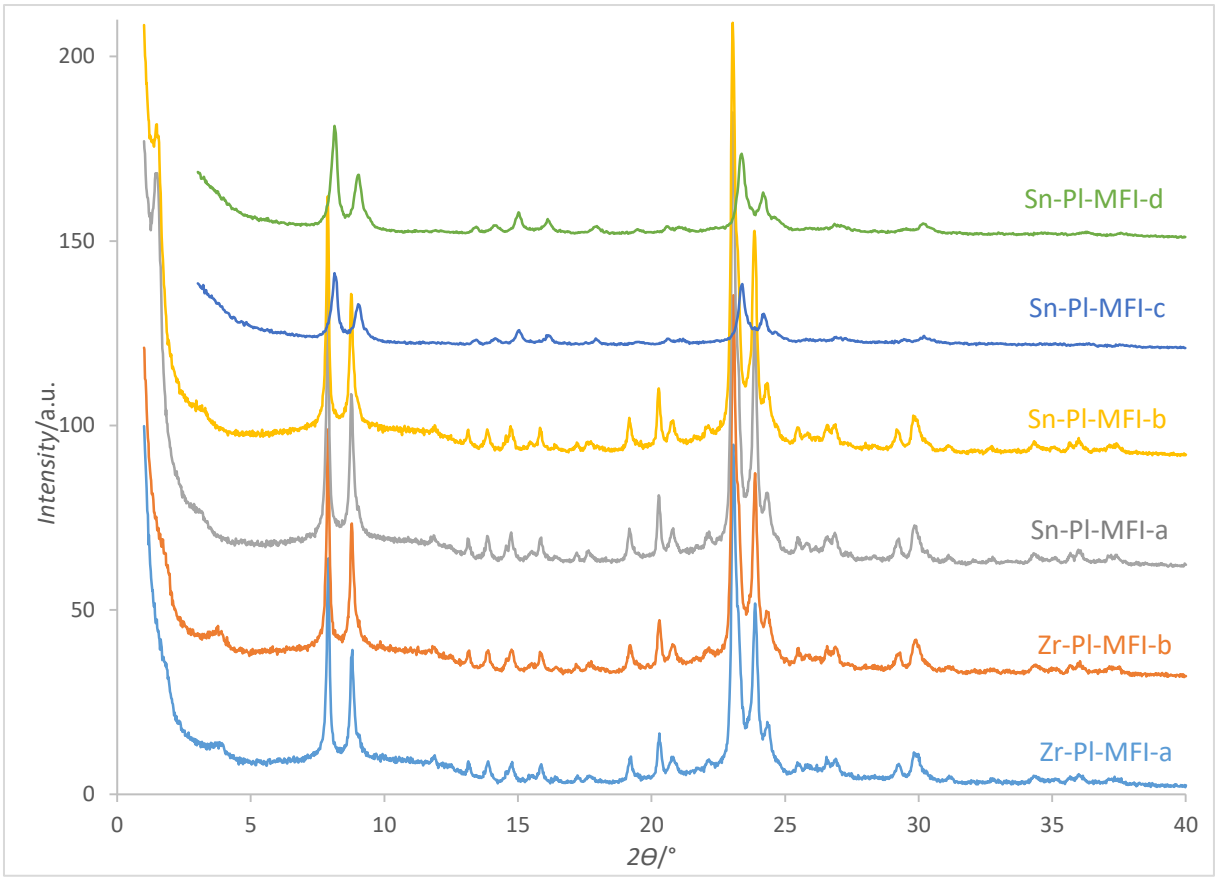

Figure 8: XRD patterns of the synthesised 2D zeolites.

Textural properties of zeolites such as surface area and pore volume are crucial for determining their use. They can be derived from the nitrogen adsorption isotherm. The textural properties of the synthesised samples are listed in Table 2. The highest BET areas (493 resp. 483 m^2/g) are observed for imp-Sn-BEA and Sn-Pl-MFI-d, while the majority of pillared samples display lower BET area (109 and 258 m^2/g for Zr-Pl-MFI-a, Zr-Pl-MFI-b, respectively, and 321 and 216 m^2/g for Sn-Pl-MFI-a, Sn-Pl-MFI-b, respectively). While the highest external surface area belongs to both Sn pillared catalysts (284 m^2/g for Sn-Pl-MFI-a and 253 m^2/g for Sn-Pl-MFI-c), the Zr pillared catalysts exhibit low external area (90 m^2/g for Zr-Pl-MFI-a and 109 m^2/g for Zr-Pl-MFI-b. The small external surface may be caused by high reactivity of Zr-isopropoxide, which readily reacts with TEOS and surface silanol groups of the layers and forms thicker pillars that fill out the interlayer space resulting in a decrease of the surface area and pore volume. On the other hand, Sn-isopropoxide has low solubility in TEOS and thus it reacts slowly as well as the TEOS itself. Therefore a smaller amount of pillars is formed. Total pore volume (0.424 and 0.415 cm^3/g respectively) follows a similar trend to BET area – Sn-Pl-MFI-d having the highest volume together with Sn-MFI-b. The highest micropore volumes (0.178 and 0.170 cm^3/g respectively) belong to imp-Sn-BEA and Zr-BEA. Low micropore

volume of pillared catalysts (0.007 and 0.067 cm^3/g for Zr-Pl-MFI-a, Zr-Pl-MFI-b and 0.015 and 0.001 cm^3/g for Sn-Pl-MFI-a, Sn-Pl-MFI-b, respectively) may be caused by a partial clogging of pores during the pillaring process. Furthermore, if amorphous silica is added in the form of pillars, the mass of the catalyst increases, while the micropore volume does not change, thus the specific micropore volume decreases.

Table 2: Textural properties and metal content of the synthesised zeolites.

	Si/M	*BET* / m^2/g	S_{ext} / m^2/g	V_{tot} / cm^3/g	V_{micro} / cm^3/g
Zr-BEA	100	473	104	0.273	0.170
Sn-BEA	96	-	-	-	-
imp-Sn-BEA	20	493	105	0.247	0.178
Zr-MFI	19	478	153	0.304	0.149
Sn-MFI-a	68	329	88	0.247	0.113
Sn-MFI-b	28	442	153	0.415	0.135
Zr-Pl-MFI-a	17	109	90	0.123	0.007
Zr-Pl-MFI-b	19	258	109	0.189	0.067
Sn-Pl-MFI-a	276	321	284	0.224	0.015
Sn-Pl-MFI-b	170	216	204	0.148	0.001
Sn-Pl-MFI-c	33	466	253	0.400	0.097
Sn-Pl-MFI-d	91	483	250	0.424	0.108

The content of Sn and Zr in zeolites is given as Si/M molar ratio in Table 2. All measured Si/M ratios differ from these Si/M in synthesis gels. Whereas Zr-BEA has the Si/M = 100, its synthesis gel contained double amount of Zr (Si/M = 50). It is challenging to obtain Si/M<100 when preparing zeolite beta and may lead to long synthesis times (up to 60 days). Zr-MFI and Sn-MFI had both Si/M = 100 in the synthesis mixture. However, Zr (IV) isopropoxide incorporates more easily than Sn (IV) chloride pentahydrate, thus the resulting Si/Zr = 19 and Si/Sn = 68. Similarly, the pillaring mixture of both Zr-Pl-MFI-a and Sn-Pl-MFI-a had the Si/M = 30 and the pillaring mixture of both Zr-Pl-MFI-b and Sn-Pl-MFI-b had the Si/M = 60. The measured Si/M ratios of Zr-Pl-MFI-a and Zr-Pl-MFI-b were significantly lower due to high solubility of Zr (IV) isopropoxide in TEOS. On the other hand, Sn (IV) isopropoxide has low solubility in TEOS and the final Si/Sn ratios are higher than expected.

UV-Vis spectra shown in Figure 9 and Figure 10 verify the incorporation of the metals into the zeolite framework and identify the presence of SnO_2 or ZrO_2. Framework tetrahedrally coordinated Zr species absorb at 205-215 nm, while ZrO_2 has an absorption maximum at ~240 nm.[34] Tetrahedrally coordinated Sn absorbs at ~ 220 nm, whereas SnO_2 has an absorption maximum at 260-280 nm.[33] The spectrum of Zr-BEA (Figure 9) has a broad band at ~210 nm confirms the incorporation of Zr into the framework. Furthermore, there is also an absorption maximum at ~ 250 nm that indicates the presence of ZrO_2. This is in accordance with observation in the IR spectrum (Figure 11). Similarly, Sn-BEA (Figure 9) absorbs at ~215 nm, which corresponds to tetrahedrally coordinated Sn in the framework. However, a broad band at ~250 nm points to presence of SnO_2, which was confirmed by the IR spectrum. Zr-MFI (Figure 9) absorbs only at 205 nm, which verifies the exclusive presence of tetrahedrally coordinated Zr species. On the other hand, Sn-MFI-a (Figure 9) has an absorption maximum at ~215 nm which corresponds to tetrahedrally incorporated Sn, and an absorption band at ~250 nm which indicates the formation of SnO_2. The spectrum of Sn-MFI-b (Figure 9) shows a peak at ~220 nm that confirms the incorporation of Sn into the framework and a second peak at ~255 nm that indicates the presence of SnO_2.

For both Zr-Pl-MFI-a and Zr-Pl-MFI-b (Figure 10), an absorption maximum at ~220 nm that confirms the incorporation of Zr into the framework is observed. The catalysts also absorb at ~250 nm due to the presence of ZrO_2. All three Sn-Pl-MFI-a, Sn-Pl-MFI-b and Sn-Pl-MFI-d absorb at ~220 nm because of tetrahedrally coordinated Sn species. However, absorption at ~ 250 nm corresponding to SnO_2, was detected only in Sn-Pl-MFI-b and Sn-Pl-MFI-d. At least partial incorporation of Sn and Zr into the zeolite framework was confirmed in all samples. The intensities of the absorption bands are proportional to the amount of particular species. Therefore, samples can be qualitatively compared between each other. However, the absolute number of particular species cannot be determined since their extinction coefficients are unknown. The wide distribution of metal species in the pillared catalysts results from the post-synthesis metal incorporation, which likely leads to the formation of more complex species, e.g., single-atom framework attached species, similarly to the case of silica-titania pillaring.[46]

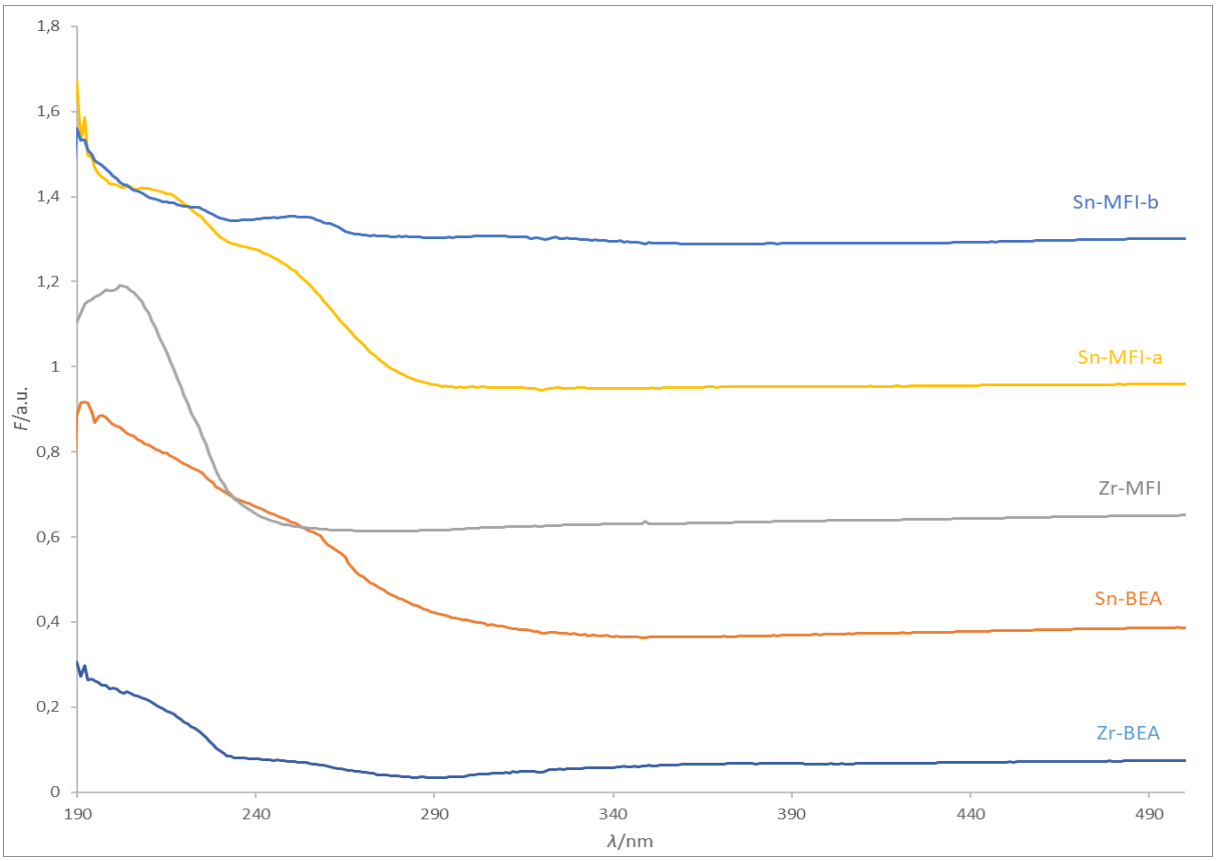

Figure 9: UV-Vis spectra of synthesised 3D zeolites.

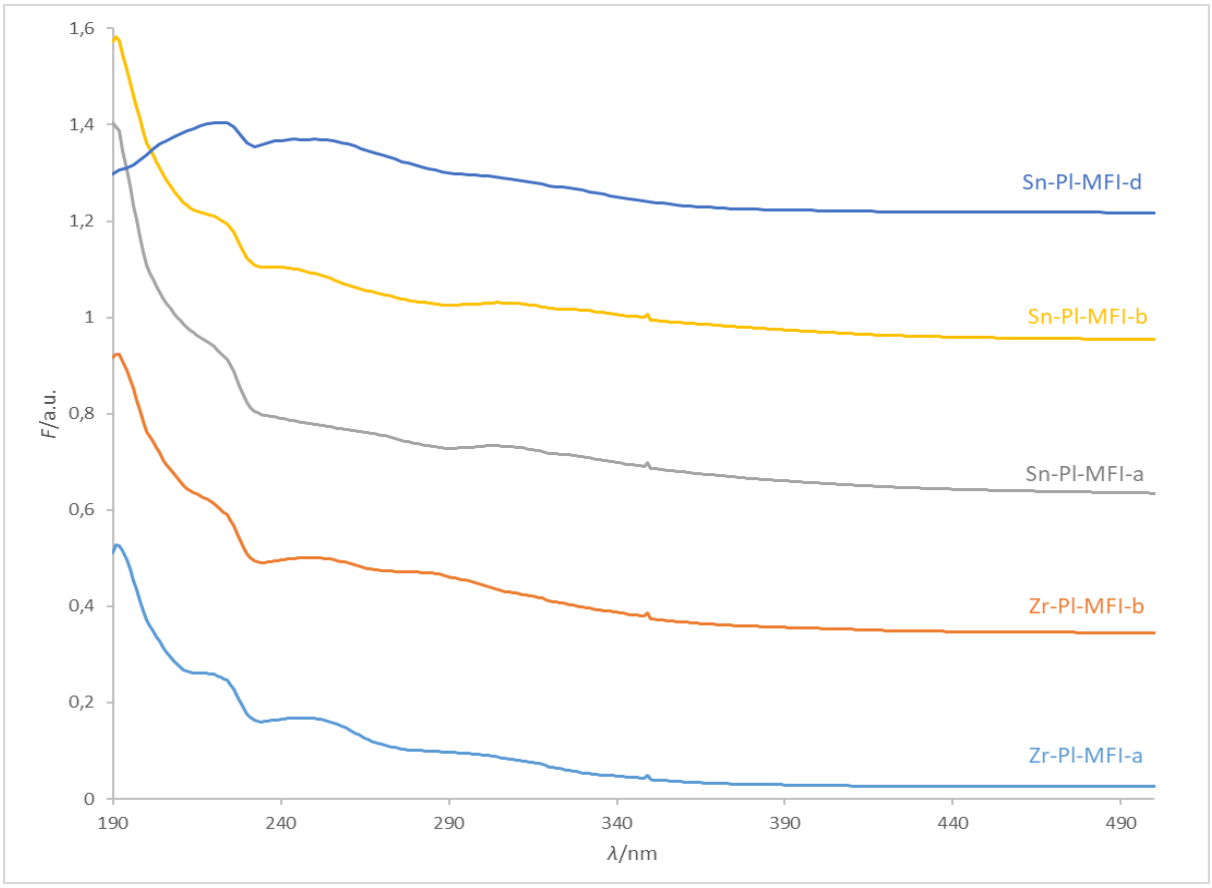

Figure 10: UV-Vis spectra of synthesised pillared zeolites.

The amount of silanol groups on the surface of selected zeolites was quantified using FT-IR. The obtained IR spectra of selected catalysts (Figure 11) contain information about the nature of silanol groups on the catalyst surface, as well as indicate the presence of ZrO_2 and SnO_2 in some cases. The peak at 1718 cm^{-1} confirms the formation of ZrO_2 in Zr-BEA and SnO_2 in Sn-BEA what is consistent with UV-Vis spectra (Figure 9). The broad band at 3505 cm^{-1} indicates the presence of oriented silanol groups connected with hydrogen bonds. These were particularly observed in Sn-MFI-b and Zr-Pl-MFI-a. The last silanol group in such oriented chain exhibits a special band at 3723 cm^{-1} corresponds to the terminal silanol. The peak at 3723 cm^{-1} is found in the spectra of Sn-MFI-b and Zr-Pl-MFI-a, which coincides with the detected silanol nests. The peak at 3745 cm^{-1} belongs to free silanol groups that are not a part of silanol nests and do not interact with any other groups.[37,38] The zeolites can be ordered according to the decreasing amount of silanol groups as Sn-Pl-MFI-c > Zr-Pl-MFI-a > Zr-BEA > Sn-MFI-b > Sn-BEA.

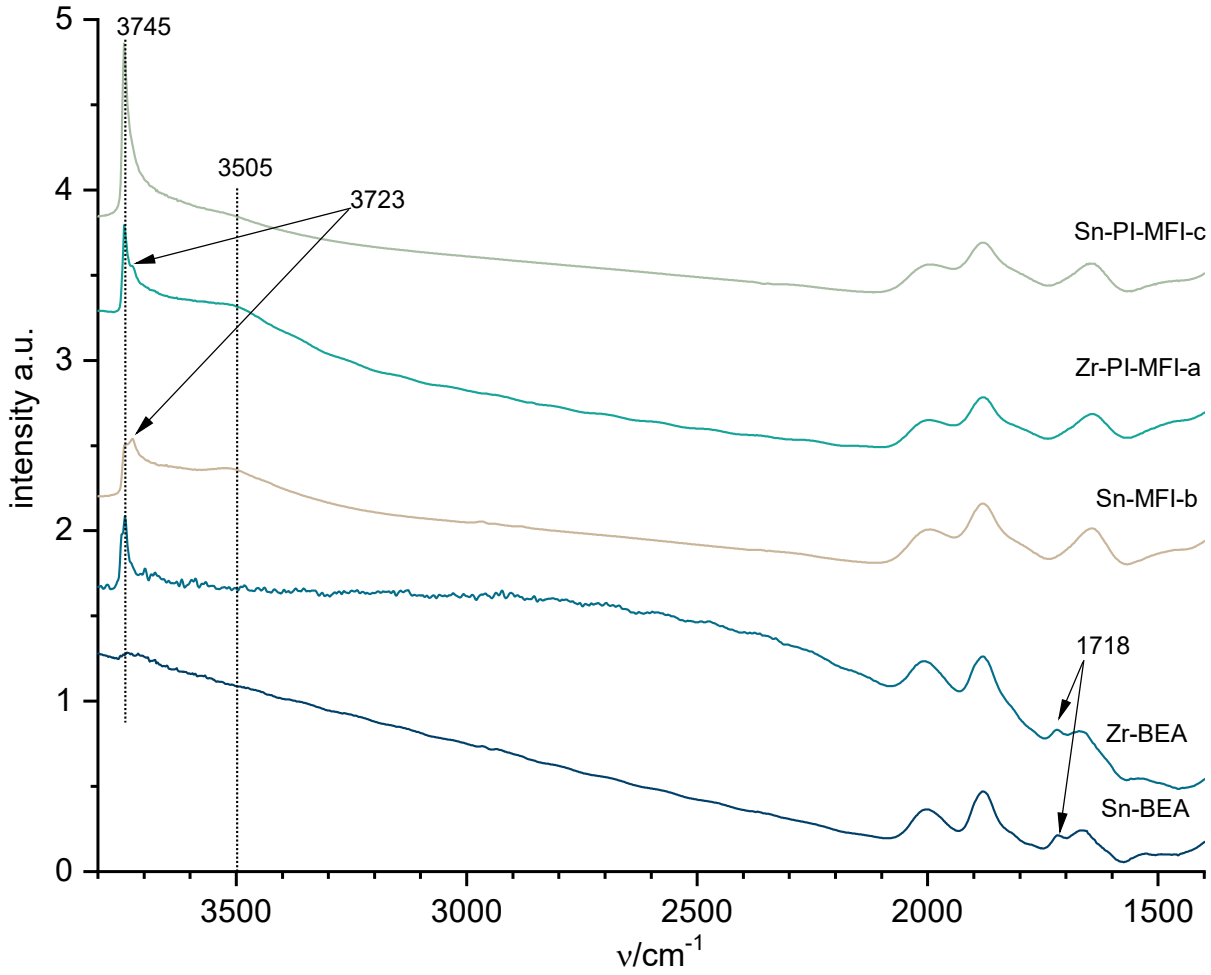

Figure 11: The infrared spectra of selected catalysts; spectra are offset.

5.2 Catalytic experiments

The synthesised catalysts were tested in MPV reduction of furfural and citronellal with isopropyl alcohol. The catalytic experiments were performed at 70 °C. The substrate/catalyst mass ratio was 2.5 and 4 in case of furfural and citronellal, respectively. The alcohol/aldehyde molar ratio was 32. The investigated Sn and Zr containing catalysts may be divided into 2 main groups - 2D (layered) zeolites and 3D (conventional) zeolites. 3D zeolites, namely large-pore zeolite beta and medium-pore zeolite MFI, were compared to 2D zeolites. The 2D catalysts were prepared by silica metal-oxide pillaring of parent layered pure-Si MFI.

A representative conversion curve of furfural over Zr-BEA is shown in Figure 12. The conversion of furfural after 4 h using all the catalysts is compared in Figure 13. The highest conversion (42 % after 4 h) was reached using the Zr-BEA as a catalyst. Other catalysts, both 3D and 2D, showed a lower conversion, which does not change in time after the first 1 h of the experiment, in contrast to Zr-BEA. The smaller pore size may cause diffusion problems, which lead to lower conversion. In contrast, the fact that conversion does not increase after one hour may be connected with the formation of oligomers of furfural, which then clog the pores, thus preventing the reactants to reach active sites. Although imp-Sn-BEA is also a large-pore zeolite, it provided significantly lower conversion (8 % after 4 h) than Zr-BEA. This justifies that the type of active site and the way of incorporation is decisive for the catalytic performance of the catalyst. Whereas Zr was incorporated into the framework of Zr-BEA directly during hydrothermal synthesis, Sn was incorporated into imp-Sn-BEA post-synthetically by impregnation. The lowest conversion (1 % after 4 h) was reached when using Sn-Pl-MFI-d. Although Sn-Pl-MFI-d has one of the highest values of textural properties (BET area = 483 m^2/g, V_{total} = 0.424 cm^3/g), it has the lowest catalytic activity from in between the synthesised catalysts. The reason is that majority of Sn is present in SnO_2, which is inactive (Figure 10). The rest of the catalysts reached conversion ranging from 8 to 14 % after 1 hour and it stayed constant until the end of the experiment. The constant value of conversion points to fast deactivation of the catalysts caused likely by the build-up of oligomers (see below). In conclusion, the pore diameter is an important factor determining the activity of a zeolite, as well as the way of Sn and Zr incorporation. Zeolites with post-synthetically incorporated Sn or Zr are not as active as Sn or Zr containing zeolites prepared hydrothermally. No straightforward correlation between textural properties or metal content can be observed.

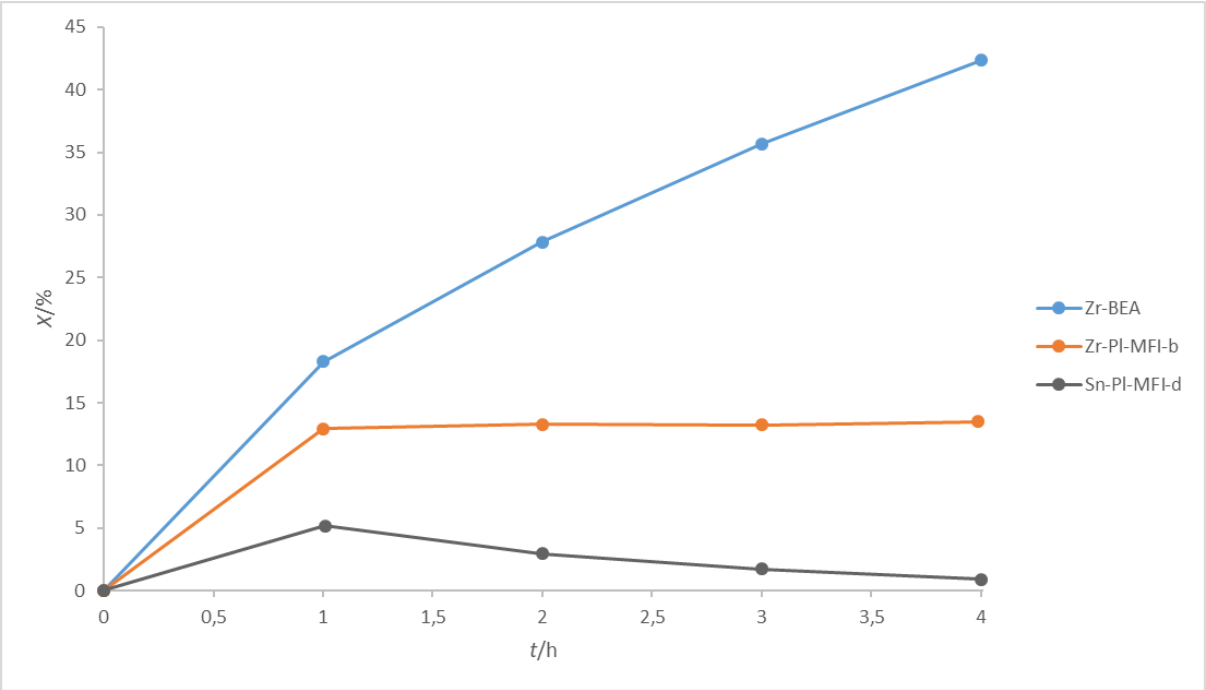

Figure 12: Conversion of furfural in MPV reduction over Zr-BEA, Zr-Pl-MFI-b and Sn-Pl-MFI-d. Reaction conditions: 100 mg catalyst, 83 mmol 2-propanol, 2.6 mmol furfural, 1.3 mmol mesitylene, 70 °C.

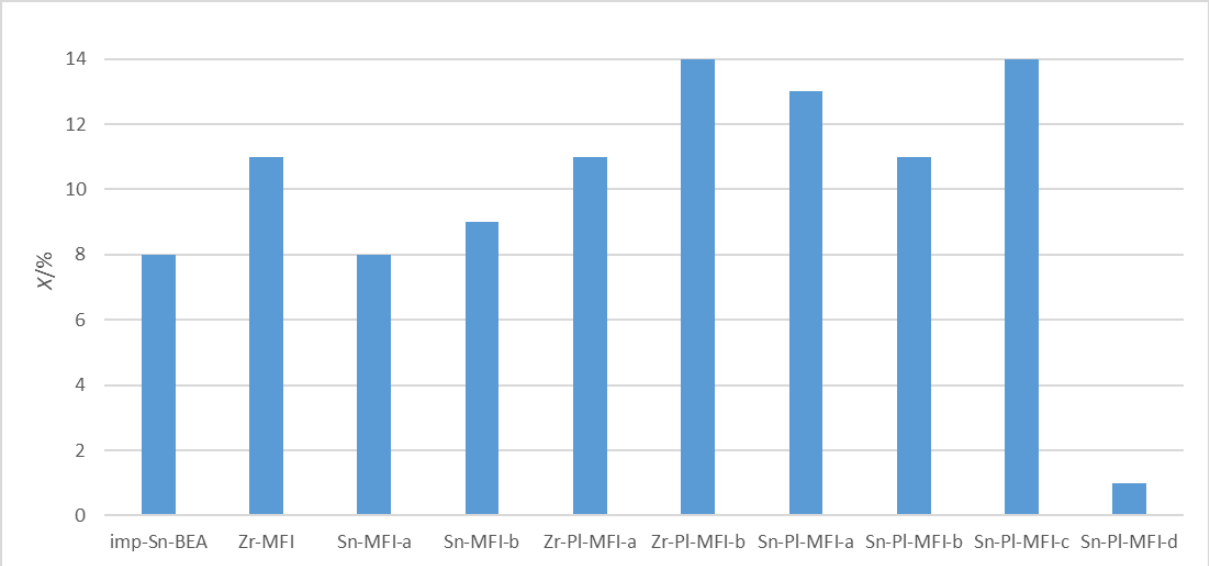

Figure 13: Conversion of furfural in MPV reduction over 3D and 2D zeolites after 4 hours. Reaction conditions: 100 mg catalyst, 83 mmol 2-propanol, 2.6 mmol furfural, 1.3 mmol mesitylene, 70 °C.

The target product of MPV reduction of furfural is furfuryl alcohol. However, formation of isopropylfurfuryl ether instead of furfuryl alcohol was observed in several cases. It was observed that Zr-BEA, Sn-MFI-a and Sn-Pl-MFI-c gave about 2 % yield of isopropylfurfuryl ether after 4 h. The yield of furfuryl alcohol follows a similar trend to that of conversion of furfural, which indicates similar selectivity of the synthesised catalysts. Zr-BEA provided the highest yield of furfuryl alcohol (35 % after 4 h), while the other catalysts provide from 0 to 4

% yield. The remaining consumed furfural was likely spent in forming oligomers, which, in turn, caused catalyst deactivation.

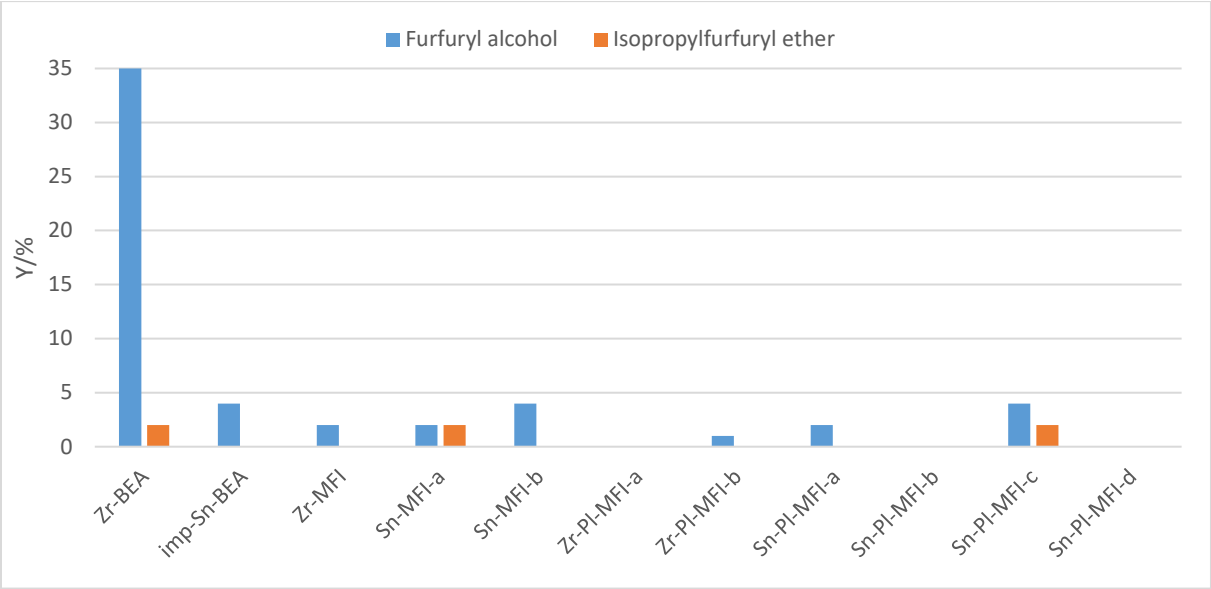

Figure 14: Yield of furfuryl alcohol and isopropylfurfuryl ether in MPV reduction of furfural after 4 hours.

The conversions of citronellal in MPV reduction are shown in Figure 15 using the 3D zeolites and in Figure 16 using the 2D catalysts. Note that all the catalysts suffered significantly less from deactivation in comparison with the above experiments with furfural. This was connected with a higher stability of citronellal against oligomerisation. The highest conversion of citronellal (52 % after 4 h) was provided by Zr-Pl-MFI-a. High activity of Zr-Pl-MFI-a may be caused by high content of Zr present in the catalyst – Si/Zr = 17. Similarly, Sn-Pl-MFI-c and Zr-Pl-MFI-b provide 44 % and 40 % conversion, respectively. On the other hand, Sn-Pl-MFI-a, Sn-Pl-MFI-b and Sn-Pl-MFI-d provide low conversion (12, 16 and 17 % after 4 h, respectively). The differences in activity result from different metal content. Whereas Sn-Pl-MFI-c and Zr-Pl-MFI-b have Si/M $\leq$ 33, the rest of the pillared catalysts have Si/M $\geq$ 91. The pillared catalysts were more active in MPV reduction of citronellal than in MPV reduction of furfural due to lack of formed oligomers, which clogged the pores of the catalysts in MPV reduction of furfural. Among the 3D catalysts, Zr-BEA gives the highest conversion of citronellal (29 % after 4 h), while Sn-BEA gives the lowest conversion (18 %). Even though Zr-BEA and Sn-BEA have the same Si/M molar ratio (100 and 96 respectively), their activity is different, suggesting that Zr containing zeolites are more active in MPV reduction than Sn containing zeolites. Sn-MFI-a was completely inactive. No conversion of citronellal is caused by the high amount of SnO_2 present in the zeolite, which is inactive in MPV reduction (cf. UV/Vis spectra, Figure 9).[2]

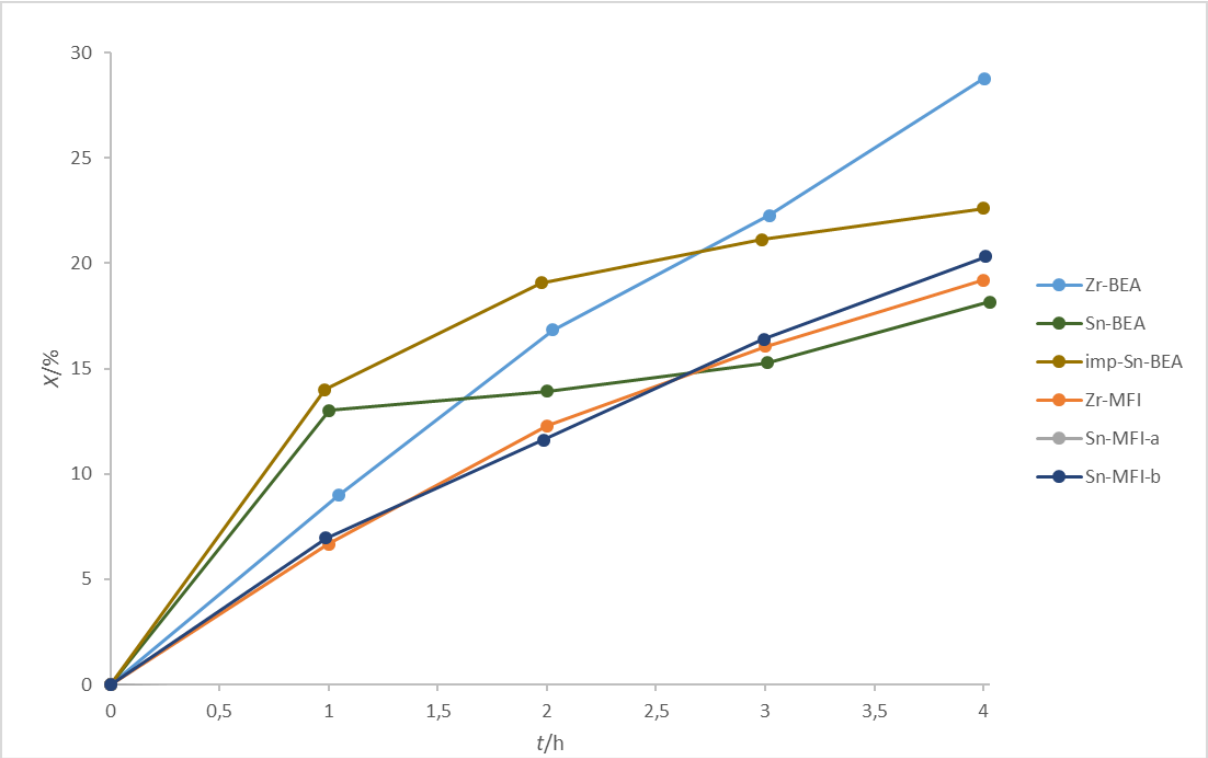

Figure 15: Conversion of citronellal in MPV reduction over 3D zeolites. Reaction conditions: 100 mg catalyst, 83 mmol 2-propanol, 2.6 mmol citronellal, 1.3 mmol mesitylene, 70 °C.

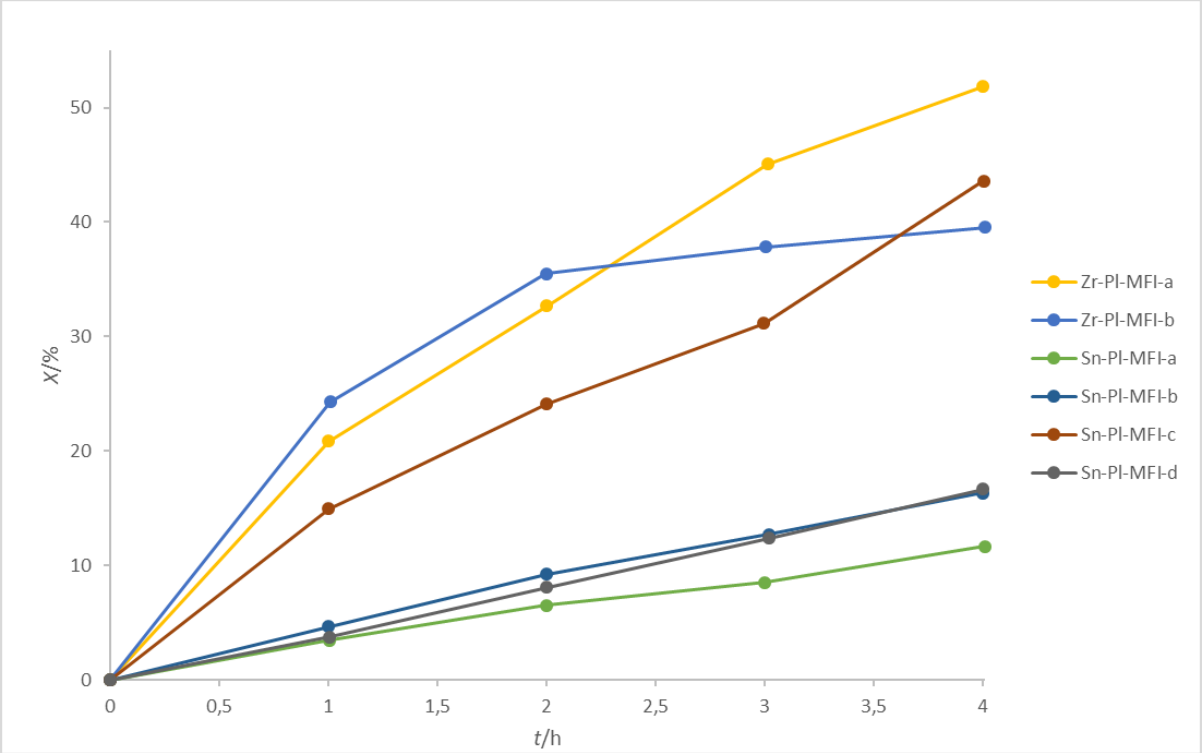

Figure 16: Conversion of citronellal in MPV reduction over 2D zeolites. Reaction conditions: 100 mg catalyst, 83 mmol 2-propanol, 2.6 mmol citronellal, 1.3 mmol mesitylene, 70 °C.

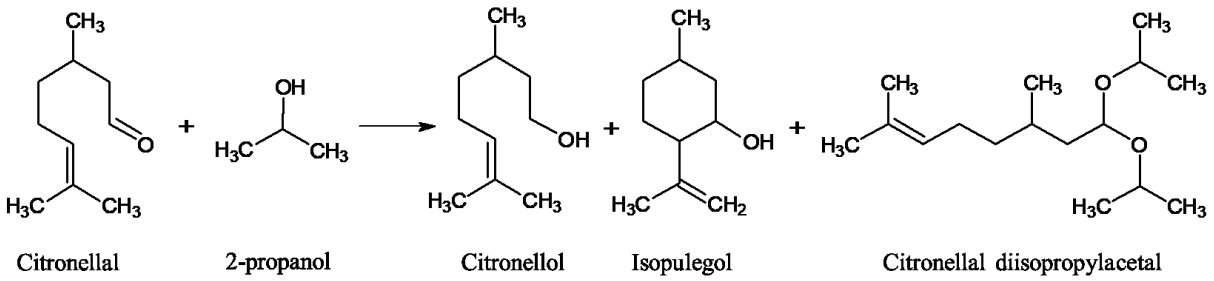

Scheme 1: MPV reduction of citronellal.

Similarly to MPV reduction of furfural, several byproducts are formed in MPV reduction of citronellal (Scheme 1). Besides the target product – citronellol – high yields of isopulegol and citronellal diisopropylacetal were detected (Figure 17). The highest yield of citronellol (28 and 9 % after 4 h, respectively) was achieved by hydrothermally synthesised Zr-BEA and Sn-BEA. On the contrary, imp-Sn-BEA with post synthetically incorporated Sn exhibited a low yield (1 % after 4 h) of citronellol. Products of acetalisation were detected when using all prepared catalysts except Zr-BEA. The amount of citronellal diisopropylacetal formed correlates with the amount of silanol groups in Zr and Sn containing zeolites (Figure 11). However, when using pure-Si MFI as a catalyst in MPV reduction of citronellal, the amount of acetalisation products does not correlate to the amount of silanol groups. Thus acetalisation is not catalysed by silanol groups alone. The combination of silanol groups and isolated Sn-OH and Zr-OH groups likely has a synergistic effect on the acetalisation. The formation of isopulegol is favoured when using Sn-BEA and imp-Sn-BEA (42 and 70 % yield after 4 h), as well as when using Zr-Pl-MFI-a and Zr-Pl-MFI-b (71 and 31 % yield after 4 h).

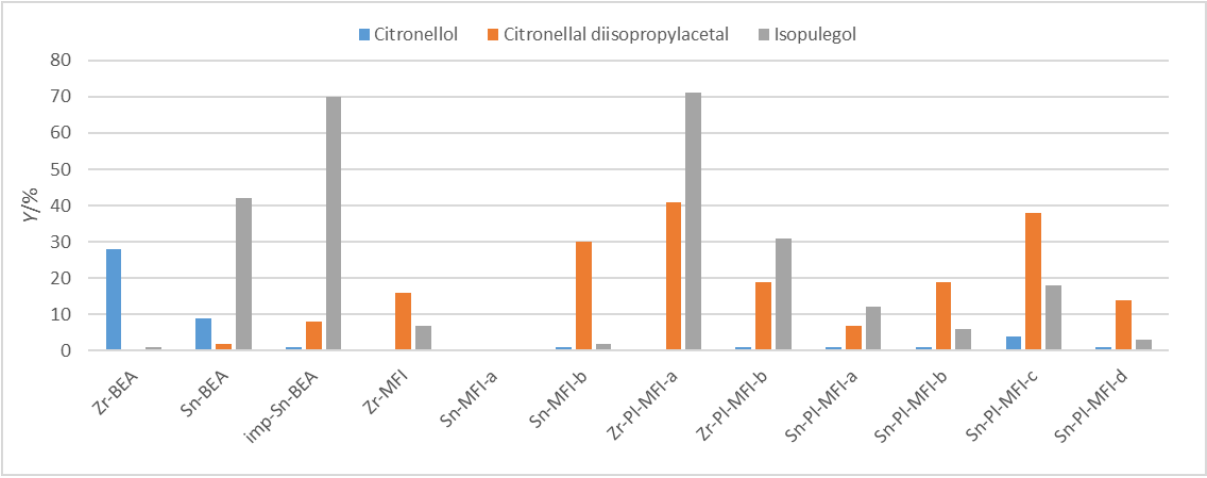

Figure 17: Yield of citronellol, citronellal diisopropylacetal and isopulegol in MPV reduction of citronella after 4 hours.

6 Conclusions

Conventional 3D zeolites with MFI and BEA topology and 2D pillared MFI zeolites were studied in MPV reduction of furfural and citronellal. The 2D catalysts (Zr-Pl-MFI-a, Zr-Pl-MFI-b, Sn-Pl-MFI-a, Sn-Pl-MFI-b, Sn-Pl-MFI-c and Sn-Pl-MFI-d) were prepared by pillaring a lamellar pure-Si MFI with mixtures of TEOS and Sn or Zr (IV) isopropoxide in various ratios. Zr-BEA, Sn-BEA, Zr-MFI, Sn-MFI-a and Sn-MFI-b were synthesised hydrothermally. Imp-Sn-BEA was prepared by degermanation, followed by impregnation of the zeolite with $SnCl_4$.

The metal incorporation was confirmed by UV-Vis spectroscopy (Figure 9 and Figure 10). UV-Vis spectroscopy, as well as FT-IR (Figure 11), detected the formation of SnO_2 and ZrO_{2i} n Zr-BEA, Sn-BEA, Sn-MFI-a, Sn-MFI-b, Zr-Pl-MFI-a, Zr-Pl-MFI-b and Sn-Pl-MFI-b. The Si/M molar ratio varies from 17 to 276 (Table 2), depending on the amount of Sn or Zr source in the synthesis gel or pillaring mixture. The textural properties of the prepared zeolites are listed in Table 2. Imp-Sn-BEA has the highest BET area (493 m^2/g) and V_{micro} (0.178 cm^3/g), while the highest S_{ex} (284 m^2/g) belongs to Sn-Pl-MFI-a and the highest V_{tot} (0.424 cm^3/g) to Sn-Pl-MFI-d.

In the MPV reduction of furfural, Zr-BEA gave the highest conversion (42 %) as well as the highest yield of furfuryl alcohol (35 %). Overall the activity depends on the pore diameter and the way of metal incorporation. Zeolites beta (6.4 Å pore diameter) gave higher conversions than MFI zeolites (5.6 Å diameter). Smaller pores can get clogged with furfural oligomers or tar faster than bigger pores and even the use of 2D zeolites did not slow down this deactivation.

In the MPV reduction of citronellal, the highest conversion (52 %) was provided by Zr-Pl-MFI-a. The highest yield of citronellol (28 %) was given by Zr-BEA as in the case with MPV reduction of furfural. Overall the activity depends on the pore diameter, the way of metal incorporation and metal content. Zeolites beta (6.4 Å pore diameter) gave higher conversions than MFI zeolites (5.6 Å diameter). Smaller pores can get clogged with furfural oligomers or tar faster than bigger pores.

In conclusion, the pillared catalysts did not facilitate the MPV reduction as expected. Although Zr-Pl-MFI-a, Zr-Pl-MFI-b and Sn-Pl-MFI-c gave higher conversion of citronellal (52, 40 and 44 %) than Zr-BEA (29 %). Zr-BEA gave the highest conversion of furfural (42 %). Moreover, Zr-BEA provided the highest yields of the desired products in both MPV

reductions (35 % for furfuryl alcohol and 28 % for citronellol). Furthermore, the activity of the pillared catalyst depends on the metal content – the lower the Si/M molar ratio, the higher the conversion.

Finally, the Zr containing catalyst showed to be more active in MPV reduction than Sn containing zeolites. Zr-BEA had higher conversion (42 % for furfural and 29 % for citronellal) in both MPV reductions of furfural and citronellal than Sn-BEA (18 % for citronellal) and imp-Sn-BEA (8 % for furfural and 23 % for citronellal). Also, the yield of the desired products was the highest for Zr-BEA (35 % for furfuryl alcohol and 28 % for citronellol).

7 References

1. Zhu, Y., Chuah, G. & Jaenicke, S. Chemo- and regioselective Meerwein-Ponndorf-Verley and Oppenauer reactions catalyzed by Al-free Zr-zeolite beta. *J. Catal.* **227**, 1–10 (2004).

2. Corma, A., Domine, M. E., Nemeth, L. & Valencia, S. Al-free Sn-Beta zeolite as a catalyst for the selective reduction of carbonyl compounds (Meerwein-Ponndorf-Verley Reaction). *J. Am. Chem. Soc.* **124**, 3194–3195 (2002).

3. Wang, J., Okumura, K., Jaenicke, S. & Chuah, G. K. Post-synthesized zirconium-containing Beta zeolite in Meerwein-Ponndorf-Verley reduction: Pros and cons. *Appl. Catal. A Gen.* **493**, 112–120 (2015).

4. Ferrini, P. *et al.* Lewis acid catalysis on single site Sn centers incorporated into silica hosts. *Coord. Chem. Rev.* **343**, 220–255 (2017).

5. Laidler, K. J. A Glossary of Terms Used in Chemical Kinetics, Including Reaction Dynamics. *Pure Appl. Chem.* **68**, 149–192 (1996).

6. Nilsson, A., Pettersson, L. G. M. & Norskov, J. (Eds.). *Chemical Bonding at Surfaces and Interfaces*. (Amsterdam, Elsevier Science, 2008).

7. Doornkamp, C. & Ponec, V. The universal character of the Mars and Van Krevelen mechanism. *J. Mol. Catal. A Chem.* **162**, 19–32 (2000).

8. Friend, C. M. & Xu, B. Heterogeneous catalysis: A central science for a sustainable future. *Acc. Chem. Res.* **50**, 517–521 (2017).

9. Cohen, R., Graves, C. R., Nguyen, S. B. T., Martin, J. M. L. & Ratner, M. A. The mechanism of aluminum-catalyzed Meerwein-Schmidt-Ponndorf-Verley reduction of carbonyls to alcohols. *J. Am. Chem. Soc.* **126**, 14796–14803 (2004).

10. Verley, A. Exchange of funtional groups between two molecules. Exchange of alcohol and aldehyde groups. *Bull. Soc. Chim. Fr.* **37**, 537–542 (1925).

11. de Graauw, C. F., Peters, J. A., van Bekkum, H. & Huskens, J. Meerwein-Ponndorf-Verley Reductions and Oppenauer Oxidations: An Integrated Approach. *Synthesis (Stuttg).* **10**, 1007–1017 (1994).

12. Moulton, W. N., Van Atta, R. E. & Ruch, R. R. Mechanism of the Meerwein-Ponndorf-Verley Reduction. *J. Org. Chem.* **26**, 290–292 (1961).

13. Ashby, E. C. Single-Electron Transfer, a Major Reaction Pathway in Organic Chemistry. An Answer to Recent Criticisms. *Acc. Chem. Res.* **21**, 414–421 (1988).

14. Boronat, M., Corma, A. & Renz, M. Mechanism of the Meerwein - Ponndorf - Verley - Oppenauer (MPVO) redox equilibrium on Sn- and Zr - Beta zeolite catalysts. *J. Phys. Chem. B* **110**, 21168–21174 (2006).

15. Van Der Waal, J. C., Creyghton, E. J., Kunkeler, P. J., Tan, K. & Van Bekkum, H. Beta-type zeolites as selective and regenerable catalysts in the Meerwein-Ponndorf-Verley reduction of carbonyl compounds. *Top. Catal.* **4**, 261–268 (1997).

16. Csicsery, S. M. Shape-selective catalysis in zeolites. *Zeolites* **4**, 202–213 (1984).

17. Roth, W. J., Nachtigall, P., Morris, R. E. & Jir, C. Two-Dimensional Zeolites : Current Status and Perspectives. *Chem. Rev.* **114**, 4807–4837 (2014).

18. Čejka, J. & Žilková, N. Syntéza a Struktura Zeolitú. *Chem. List.* **94**, 278–287 (2000).

19. Do, D. M., Jaenicke, S. & Chuah, G. K. Mesoporous Zr-SBA-15 as a green solid acid catalyst for the Prins reaction. *Catal. Sci. Technol.* **2**, 1417–1424 (2012).

20. Corma, A., Navarro, M. T. & Renz, M. Lewis acidic Sn(IV) centers - Grafted onto MCM-41 - As catalytic sites for the Baeyer-Villiger oxidation with hydrogen peroxide. *J. Catal.* **219**, 242–246 (2003).

21. Li, P. *et al.* Postsynthesis and selective oxidation properties of nanosized Sn-beta zeolite. *J. Phys. Chem. C* **115**, 3663–3670 (2011).

22. Hammond, C., Conrad, S. & Hermans, I. Simple and scalable preparation of highly active lewis acidic Sn-β. *Angew. Chemie - Int. Ed.* **51**, 11736–11739 (2012).

23. Přech, J., Eliášová, P., Aldhayan, D. & Kubů, M. Epoxidation of bulky organic molecules over pillared titanosilicates. *Catal. Today* **243**, 134–140 (2015).

24. Choi, M. *et al.* Stable single-unit-cell nanosheets of zeolite MFI as active and long-lived catalysts. *Nature* **461**, 246–249 (2009).

25. Roth, W. J. *et al.* Postsynthesis transformation of three-dimensional framework into a lamellar zeolite with modifiable architecture. *J. Am. Chem. Soc.* **133**, 6130–6133 (2011).

26. Eliášová, P. & Čejka, J. Two-dimensional Zeolites. In: *Zeolites in Catalysis: Properties and Applications.* Čejka, J., Morris, R. E. & Nachtigall, P. (Eds.) (Croydon: The Royal Society of Chemistry, 2017) p. 146–193.

27. IZA Database: *Database of Zeolite Structures*. Available at URL: <http://www.iza-structure.org/databases/> [cit. 18.06.2021].

28. Lu, T., Yan, W. & Xu, R. Chiral zeolite beta: structure, synthesis, and application. *Inorg. Chem. Front.* **6**, 1938–1951 (2019).

29. Morris, R. E. & Allan, P. K. Structure Determination. In: *Zeolites in Catalysis: Properties and Applications.* Čejka, J., Morris, R. E. & Nachtigall, P. (Eds.) (Croydon, The Royal Society of Chemistry, 2017) p. 194–239.

30. Thommes, M. *et al.* Physisorption of gases, with special reference to the evaluation of surface area and pore size distribution (IUPAC Technical Report). *Pure Appl. Chem.* **87**, 1051–1069 (2015).

31. Pechoušek, J. *Měření plochy povrchu pevných látek a určování jejich porozity metodou sorpce plynu*. Available at URL: <https://fyzika.upol.cz/cs/system/files/download/vujtek/ostatni/BET.pdf> [cit. 18.06.2021].

32. Perkampus, H.-H. Recent Developments in UV-VIS Spectroscopy. In: *UV-VIS Spectroscopy and Its Applications* (Berlin, Springer, Berlin, Heidelberg, 1992) p. 81–130.

33. Wang, X. *et al.* Characterization and catalytic properties of tin-containing mesoporous silicas prepared by different methods. *J. Mol. Catal. A Chem.* **238**, 185–191 (2005).

34. Morey, M. S., Stucky, G. D., Schwarz, S. & Fröba, M. Isomorphic substitution and postsynthesis incorporation of zirconium into MCM-48 mesoporous silica. *J. Phys. Chem. B* **103**, 2037–2041 (1999).

35. Zhou, W. Electron Microscopy of Zeolites. In: *Zeolites in Catalysis: Properties and*

Applications. Čejka, J., Morris, R. E. & Nachtigall, P. (Eds.) (Croydon, The Royal Society of Chemistry, 2017) p. 277–309.

36. Titus, D., James Jebaseelan Samuel, E. & Roopan, S. M. Nanoparticle characterization techniques. In: *Green synthesis, Characterization and Applications of Nanoparticles.* Shukla, A. K. & Iravani, S. (Eds.) (Amsterdam, Elsevier, 2019) p. 303–319.

37. Gallas, J.-P. *et al.* Quantification of Water and Silanol Species on Various Silicas by Coupling IR Spectroscopy and in-Situ Thermogravimetry. *Langmuir* **25**, 5825–5834 (2009).

38. Bordiga, S. *et al.* Characterisation of defective silicalites. *J. Chem. Soc. Dalt. Trans.* 3921–3929 (2000).

39. Moliner, M., Román-Leshkov, Y. & Davis, M. E. Tin-containing zeolites are highly active catalysts for the isomerization of glucose in water. *Proc. Natl. Acad. Sci.* **107**, 6164–6168 (2010).

40. Přech, J., Vitvarová, D., Lupínková, L., Kubů, M. & Čejka, J. Titanium impregnated borosilicate zeolites for epoxidation catalysis. *Microporous Mesoporous Mater.* **212**, 28–34 (2015).

41. Zhao, Z. *et al.* Hydrothermal synthesis of mesoporous zirconosilicate with enhanced textural and catalytic properties with the aid of amphiphilic organosilane. *Microporous Mesoporous Mater.* **123**, 324–330 (2009).

42. Garcia Vargas, N., Stevenson, S. & Shantz, D. F. Synthesis and characterization of tin(IV) MFI: Sodium inhibits the synthesis of phase pure materials. *Microporous Mesoporous Mater.* **152**, 37–49 (2012).

43. Mal, N. K., Ramaswamy, V., Rajamohanan, P. R. & Ramaswamy, A. V. Sn-MFI molecular sieves: Synthesis methods, 29Si liquid and solid MAS-NMR, 119Sn static and MAS NMR studies. *Microporous Mater.* **12**, 331–340 (1997).

44. Na, K., Jo, C., Kim, J., Ahn, W.-S. & Ryoo, R. MFI Titanosilicate Nanosheets with Single-Unit-Cell Thickness as an Oxidation Catalyst Using Peroxides. *ACS Catal.* **1**, 901–907 (2011).

45. Choi, M. *et al.* Stable single-unit-cell nanosheets of zeolite MFI as active and long-

lived catalysts. *Nature* **461**, 246-249 (2009).

46. Přech, J. & Čejka, J. UTL titanosilicate: An extra-large pore epoxidation catalyst with tunable textural properties. *Catal. Today* **277**, 2–8 (2016).